SEISMIC INTERPRETATION AND 2D RESTORATION OF F-A GAS FIELD, BREDASDORP BASIN SOUTH COAST OF SOUTH AFRICA.

Zamazulu Ngejane

Mini-thesis

Supervisors:

Prof J.V. B. Donker (UWC)

Dr S. Lanes (UWC)

A mini- thesis submitted in partial fulfilment of the requirements for the degree of Magister Scientiae in the Department of Earth Sciences, University of the Western Cape.

SEISMIC INTERPRETATION AND 2D RESTORATION OF F-A GAS FIELD, BREDASDORP BASIN SOUTH COAST OF SOUTH AFRICA.

KEYWORDS

Bredasdorp Basin

South Africa

F-A gas field

Depth conversion

Structural interpretation

Pre-rift strata

Syn-rift strata

Post-rift

Decompaction

Restoration

Extensional stress

Compressional stress

Inversion

SEISMIC INTERPRETATION AND 2D RESTORATION OF F-A GAS FIELD, BREDASDORP BASIN SOUTH COAST OF SOUTH AFRICA.

ABSTRACT

Seismic interpretation is always somewhat an uncertainty and questions on whether the horizons picked are properly correlated across faults and or the structures mapped are geologically or geometrically sensible always raise a concern as it provides the principal source of subsurface information used commonly in exploration by the oil and gas industry. In this study an attempt of delineating what are or not geological features has been done by validating the seismic structural interpretation using the restoration technique which also provided information about the extensional history of the study area.

The seismic data, horizon and fault interpretation have been depth converted in 2DMove software followed by a sequential restoration and decompacting workflow. Simple shear was used as the restoration algorithm based on the deformation style of the basin (extensional basin).

The seismic interpretation is valid and studies on tectonics interplay in basin development (gas field scale) during the Late-Jurassic- Early Cretaceous are based on the results of the four balanced cross-sections. They indicate that the Basin is not a simple extensional rift Basin but was rather formed through an alternation of extensional and compressional phases.

The area understudy has undergone extension since rifting onset (break-up of Gondwana) with two intervening minor inversion episodes further NW and SE showing no significant shortening on the central part. A maximum extension is noted within the central part of the study area along the XL_1248 thus more accommodation space and subsequently thicker sediment accumulations are encountered in this region.

SEISMIC INTERPRETATION AND 2D RESTORATION OF F-A GAS FIELD, BREDASDORP BASIN SOUTH COAST OF SOUTH AFRICA.

DECLARATION

I declare that, *Seismic interpretation and 2D restoration of F-A gas field Bredasdorp Basin South Coast of South Africa* is my own work and that it has not been submitted before for any degree or examination in other universities. All sources that have been used or quoted are indicated and acknowledge by complete references.

Full name: Zamazulu Ngejane

Date :

Signed :

ACKNOWLEDGEMENT

I would like to thank Prof. Jan Van Bever Donker & Dr Silvia Lanes for their continued support throughout the research and the external supervision from Dr Antonio Ravaglia. Dr W. Sonibare has also played a huge role providing recommendations and steering on the research. Lastly I thank the PetroSA team for providing me with the necessary study material and the opportunity they granted me on working with the data from one of the producing gas fields.

TABLE OF CONTENTS

LIST OF FIGURES

LIST OF TABLES

.


UNIVERSITY of the
WESTERN CAPE
RESPICE PROSPICE

CHAPTER 1

INTRODUCTION

SEISMIC INTERPRETATION AND 2D RESTORATION OF F-A GAS FIELD, BREDASDORP BASIN SOUTH COAST OF SOUTH AFRICA.

Structural mapping is an important application in exploration as most of the world's reservoirs are located in structural highs and seismic data is the principal source of information that provides an understanding of the geometry of the subsurface geology. The interpreter needs to be knowledgeable about the subsurface formations and the stress regime as it helps in delineating what is or not a geological feature because seismic data always include defects. These defects are due to both acquisition and processing techniques resulting in multiple reflections or artefacts such as; fault shadow; migration smiles and frowns; velocity pull-up and push-down and many others flaws (Calvert, 2004).

Different approaches and philosophies (including analogues) are used in extracting subsurface geological information from seismic data. This is a critical step in the interpretation process as not everything seen on seismic imagery is geology, thus validation of the structural interpretation from seismic data is imperative as it lowers the degree of uncertainty.

Structural restoration is a well-known methodology and it was used in this study as a technique to validate structural interpretation. It allows the interpreter to assess any geological cross-section and to highlight geometric inconsistencies, it also provides information on the progressive development of the deformation as it is an important analytical tool to understand the paleo-geometry of a basin and its evolution.

The aim of this study is to provide a geometrically valid structural interpretation that is representative of the geology and to reconstruct the evolution of these structural features through time.

This will be achieved using the seismic section restoration technique outlined in Chapter 3.

BACKGROUND

The F-A, E-M and satellite gas fields (Figure 1.1) are located in Block 9 within the Bredasdorp Basin 90 km offshore south of Mossel Bay and they are owned and operated by the State's oil company PetroSA. These fields were discovered in the 1980's when exploration was most active with a total of 181 wells (Petroleum Agency SA, 2013).

The F-A gas field began producing gas and condensate in 1992 which are piped ashore to the PetroSA GTL plant located in Mossel Bay where they are converted into paraffin, petrol, diesel and petrochemicals. The E-M gas field commenced gas production in 2000. Recorded from these fields was a gas production of ~160 MMscf/d (Million standard cubic feet per day) and 3900 BOPD (barrels of oil per day) (Petroleum Agency SA, 2013).

In the late 1980's two oil fields were discovered, the Oribi and Oryx. The former began production in 1997 at an initial rate of 25000 BOPD from a floating production facility (the Orca) and in 2000 the latter was brought on-stream using the same facilities (Petroleum Agency SA, 2013).

The Sable field also within the Bredasdorp Basin discovered in 1989 was brought to production in 2003 and in 2006 the average oil production was 9700 BOPD. In 2008 oil production from the field ceased giving passage to gas production which is now the supplement feedstock to the PetroSA GTL plant (Petroleum Agency SA, 2013).

The Oribi and Oryx fields are now almost depleted with minor production and the gas fields are also in decline, thus there is a demand for exploration of domestic reserves. It is for this reason the project was set forward, to re-interpret the structural geology of the area in seeking possible new ventures or those that may have been overlooked.

The technique used in the analysis does not only validate seismic interpretation but is also used in understanding the basin development, prediction of structures and their geometry beyond available data. Figure 1.1 shows the location of the study area.

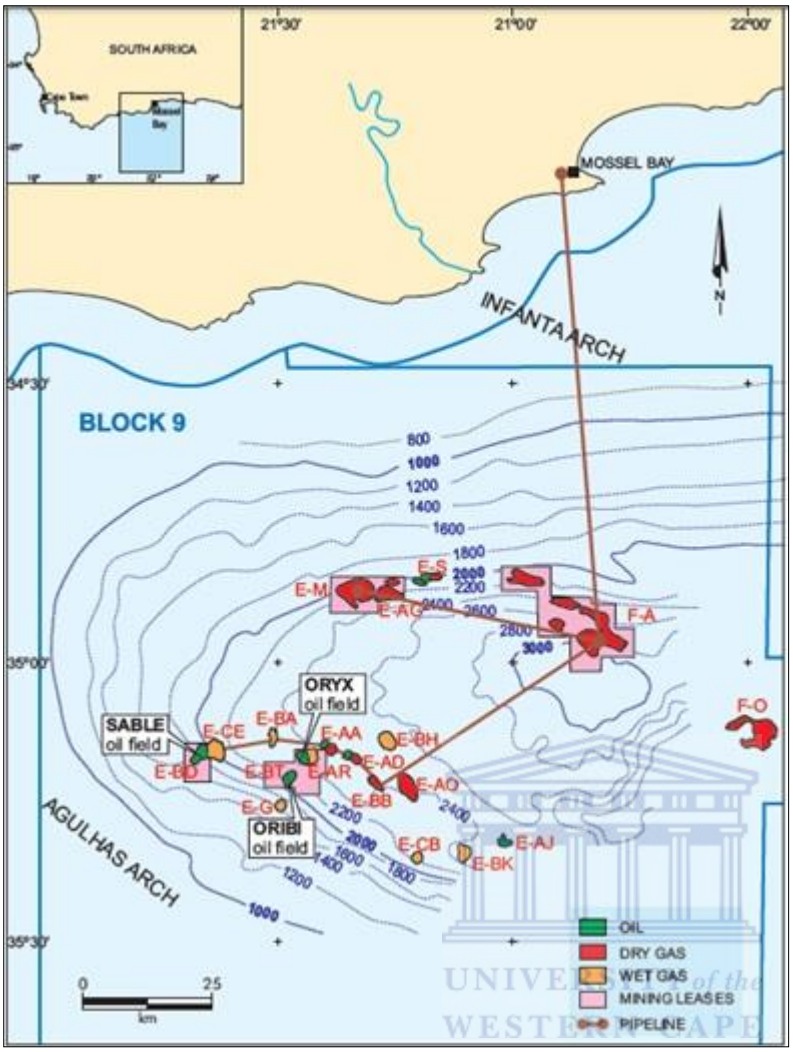

Figure 1.1 Location map of the oil and gas fields within Block 9 of the Bredasdorp Basin at 1At1 depth contours. (Petroleum Agency S.A, 2013).

LITERATURE REVIEW

The Bredasdorp Basin has undergone intensive research in characterizing the reservoir sands in the area as it has been the only hydrocarbon producing basin in the country however, the structural geology still remains somewhat an uncertainty limited by seismic image quality and the evolving seismic interpretation technologies. This has led to two contrasting models being proposed which still need to be tested for validity. A proposed Bredasdorp Basin evolution model by Du Toit (1976) recognises it to have formed in response to a single rifting event and tectonism ceased thereafter, suggesting the Basin to have subsequently developed in response to thermal subsidence with neither extension nor compression stresses recognised.

The above is contested by Van der Merwe and Fouche (1992) suggesting that the Bredasdorp Basin was formed by a complex sequence of tectonic events interpreting three compressional phases that resulted in a positive inversion with intervening extensional phases which he demonstrated on a depth-migrated 2D seismic survey (Figure 1.2).The first inversion episode is documented to have occurred pre-1At1 which is the pre-drift onset unconformity with the second occurring post-1At1 as it involves the deformation of the late Valanginian unconformity, the last recognised inversion episode occurred in Mid-Albian times.

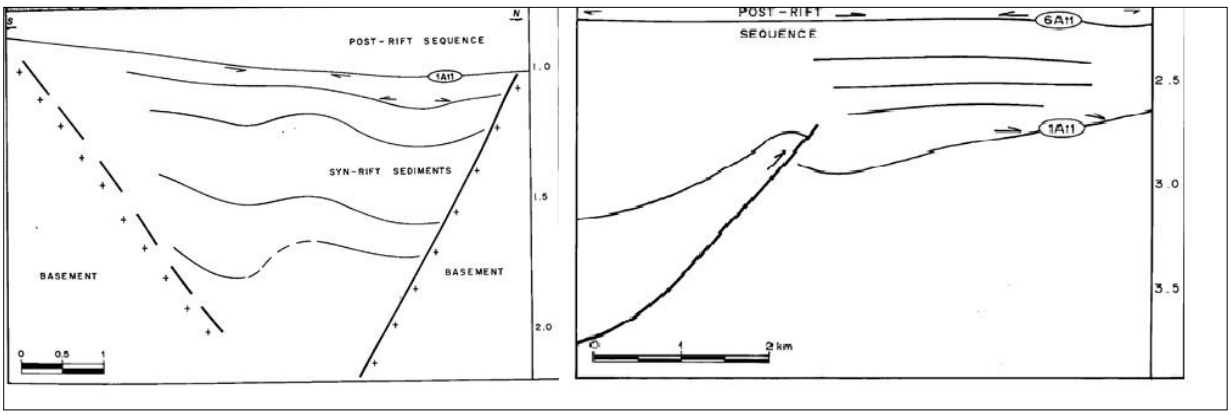

Figure 1.2. Show an inverted half-*graben* on the left which is pre-1At1 (post-rift unconformity) and the post-rift inversion on the right (Van der Merwe & Fouche, 1992).

*[1]1At1 is the break-up unconformity, a type-1 sequence boundary which marks the onset of transform motion rifting phase II

Van der Merwe and Fouche *(*1992) also described three generations of fault formation, these are listed chronologically from oldest to youngest and can also be recognised from an interpreted depth migrated seismic profile (Figure 1.2).

1. Rift faults that do not displace the drift-onset unconformity 1At1.
2. Normal faults that displace the 1At1 unconformity involving the lower sequence of the post-rift.
3. Normal faults that displace the base of the Tertiary unconformity.

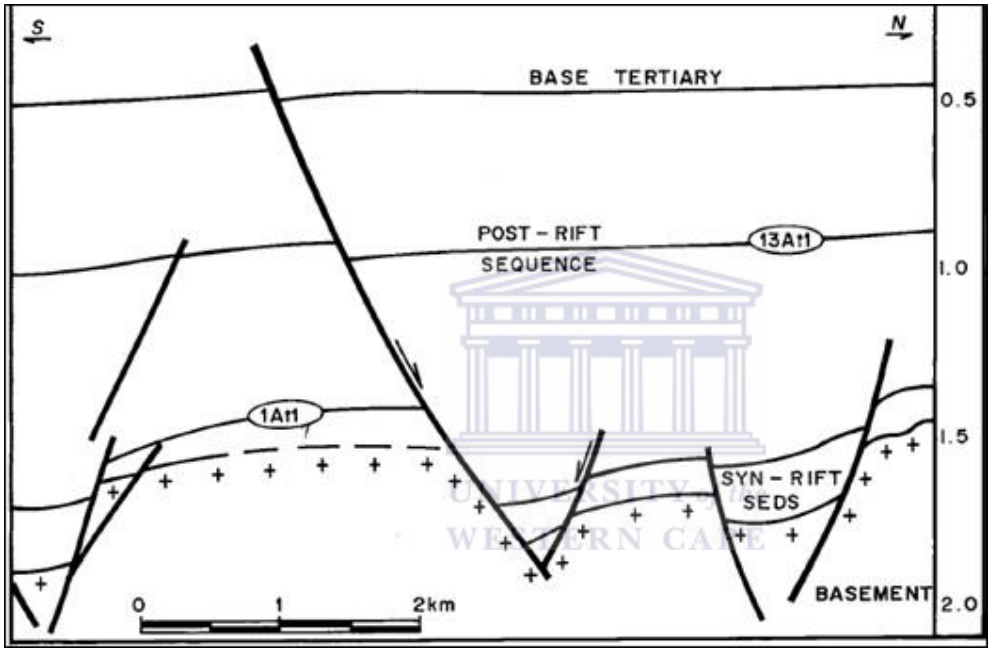

Figure 1.3. Seismic schematic in Two-way-Time (seconds) showing normal faults of different ages (Van der Merwe & Fouche, 1992).

Also described is the geometry of the normal faults which are said to be listric and detached onto a common *decollement* plane at depth, with several normal faults having associated transfer faults. This geometry is known as a linked-fault system according to Gibbs's (1984, 1989 and 1990) definition. These faults regionally show a WNW-ESE trend which is modified in the Bredasdorp Basin by trending more to the NW-SE.

Similar fault trends in this area are associated to either the drag along the Agulhus Falkland Fracture Zone (AFFZ) according to (Du Toit, 1976; Van der Merwe & Fouche, 1992) or were inherited from the Cape Fold Belt faulting according to (Cartwright, 1989).

With the provided literature it is evident that the tectonic interplay in basin development of the Bredasdorp Basin is still somewhat unclear as none of the two proposed models have been tested if they are geometrically and geologically valid or not. The above contesting models on Bredasdorp Basin evolution created a need for further studies to better understand its structural geology and evolution.

A different approach was employed to re-interpret the seismic structural geology on a field scale testing the accuracy of the proposed models.

CHAPTER 2

REGIONAL GEOLOGIC SETTING

The southernmost margin of Africa is said to have records of dextral (right lateral) shear movements (Dingle *et al.*, 1983; Van der Merwe and Fouche, 1992; Ben-Avraham *et al.*, 1997; McMillan *et al.*, 1997; Thomson, 1998; Broad *et al.*, 2006) along the Agulhas-Falkland Fracture Zone (AFFZ) where the Southern African plate rifted from the South America plate, whilst the western margin experienced a pull-apart rifting style. Rifting is said to have commenced as a preliminary fracturing of Gondwana into East Gondwana (Antarctica-India-Australia) and West Gondwana (South America-Africa), subsequently paving the way for basin opening and consequently sedimentation on the greater South Atlantic Margin and dates back from Late Mesozoic (Mid-Late Jurassic) to Early Cretaceous (Figure 2.1).

Igneous intrusion marked the beginning of the break-up of continents. Based on evidence from fission track data (Condie, 1989) as well as volcanic evidence the above is confirmed by Gilbert (1997). They also found that rifting started earlier in the east of Southern Africa at about 160± 30 Ma while in the west it is approximated to have started at about 150± 15 Ma. Crustal thinning and lithospheric stretching were succeeded by thermal subsidence which resulted in the formation of three tectonostratigraphic zones namely:

1) The eastern narrow passive margin basin formed as a result of the break-up separating Africa from Madagascar and Antarctica in the Jurassic.
2) The southern passive margin basin (Outeniqua Basin) characterised by strong strike-slip movements in the Late Jurassic to Early Cretaceous as the complex series of micro plates including the Falkland Plateau gradually moved west south-westward past the southern coast of the African margin. The Outeniqua Basin is the main result of this separation and comprises of five easterly trending *en echelon* sub-basins (Figure 2.2). The Algoa Basin formed first followed by the Gamtoos Basin, the Pletmos Basin, the Infanta Embayment and the Bredasdorp Basin respectively (Petroleum Agency SA, 2013).
3) The broad western passive margin basin (Orange Basin) related to the opening of the South Atlantic in the Early Cretaceous and was initiated as a series of linked north-

south trending *grabens* where sedimentation subsequently took place in a marginal passive marine setting (Petroleum Agency SA, 2013).

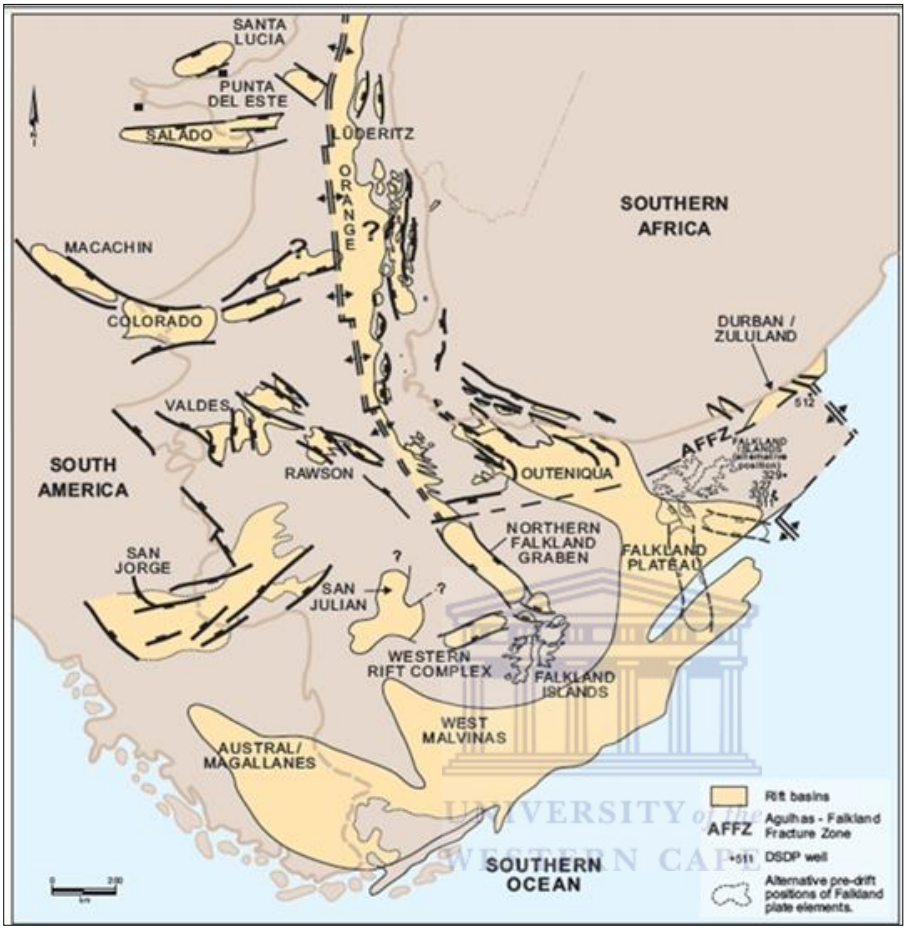

Figure 2.1 Early break-up distribution of rift basins within the southwest Gondwana, after Jungslager (1999).

THE OUTENIQUA BASIN

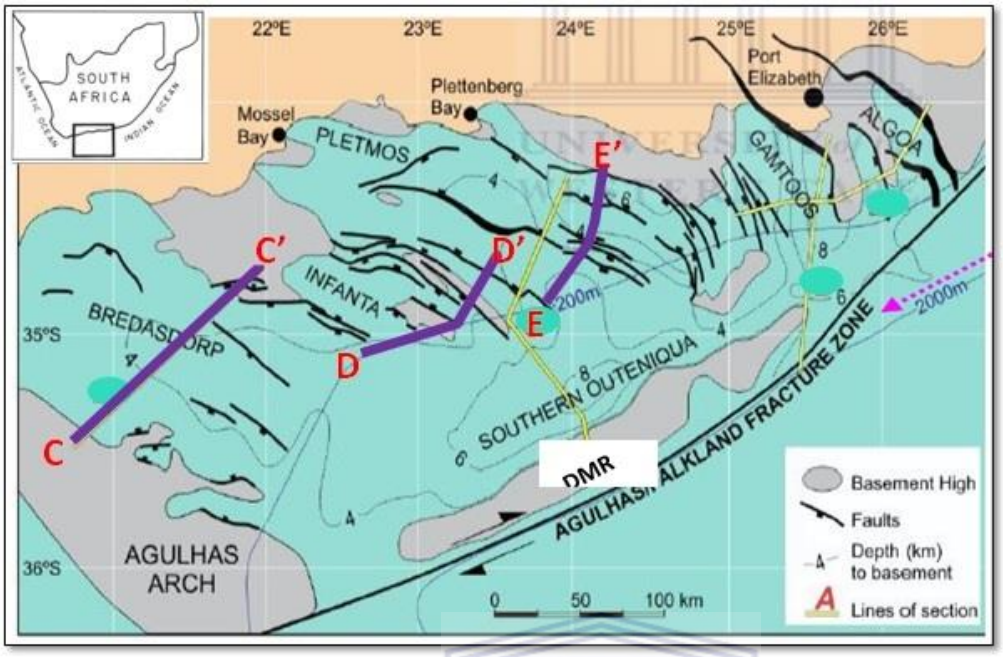

Figure 2.2 Basin location map (PASA, 2003).

The Outeniqua Basin consists of a series of listric normal faults and basement that form the boundaries between the sub-basins. The Diaz Marginal Ridge (Ben-Avraham *et al.*, 1997; DMR, Fig 2.1) bounds the sub-basins southward separating them from the AFFZ lineament.

The basement of the Outeniqua Basin is made up by the Cape Super-group rocks (sandstones and shales) deposited in the Late Palaeozoic in a retro arc foreland basin on the southern perimeter of the Kaapvaal Craton (McLachlan and McMillan, 1979; Johnson, 1991). These are overlain by the Karoo Super-group rocks on the present day onshore region but which are absent in the area under consideration due to either non-deposition or erosion as suggested by Biddle *et al* (1986) and Cole (1992).

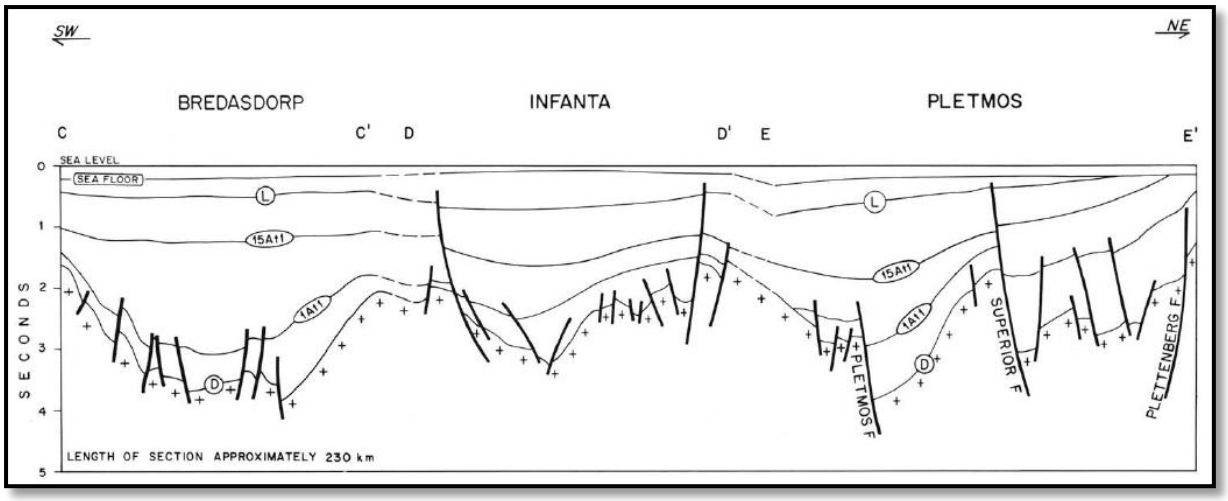

Figure 2.3. Schematic profile across Bredasdorp, Infanta and Pletmos basins, see Fig. 2.1 for profile location. The diagram shows the bounding ridges that separate the Outeniqua Basin into sub-basin after McMillan *et al* (1997).

The Cape Orogeny occurred in Permo-Triassic times when the Gondwana landmass overrode the Pacific Plate and an oblique subduction ensued (Dingle *et al*., 1983) thrusting the Cape Super group rocks and earlier depositions of the Karoo Super group. This resulted in folding and faulting and these structural grains (trending in the WNW-ESE direction) are underlying all the offshore basins of southern Africa.

LOCAL GEOLOGIC SETTING

BREDASDOPR BASIN

The Bredasdorp sub-basin (Figure 2.2) located on the southern South African Coast is a south-easterly trending rift basin covering an area of about ~16 000 km^2 (2000km long and 80 km wide) bounded by the Columbine-Agulhas arch in the southwest and Infanta arch in the northeast and which opens up to link with the adjacent Southern Outeniqua Basin in the southeast (McMillan *et al*., 1997).

The Basin infill comprises of Upper Jurassic and Lower Cretaceous syn-rift continental and marine strata and post Cretaceous and Cenozoic divergent margin strata (Brown *et al*., 1995; Turner *et al.*, 2000). The lithologies consist of Devonian black slates from the Bokkeveld Group and the Table Mountain Group quartzites which are Ordovician-Silurian in age are encountered only close to the Infanta Embayment.

Normal faults are associated with the rifting phase during the break up of Gondwana in the east causing dextral transtensional stresses in the Bredasdorp Basin trending northwest to southeast. This faulting phase resulted in *graben* and half *graben* formation which became the depo-centers within the basin (Brown *et al.*, 1995; McMillan *et al.*, 1997) bounded by arches forming structural highs (Figure 2.4).

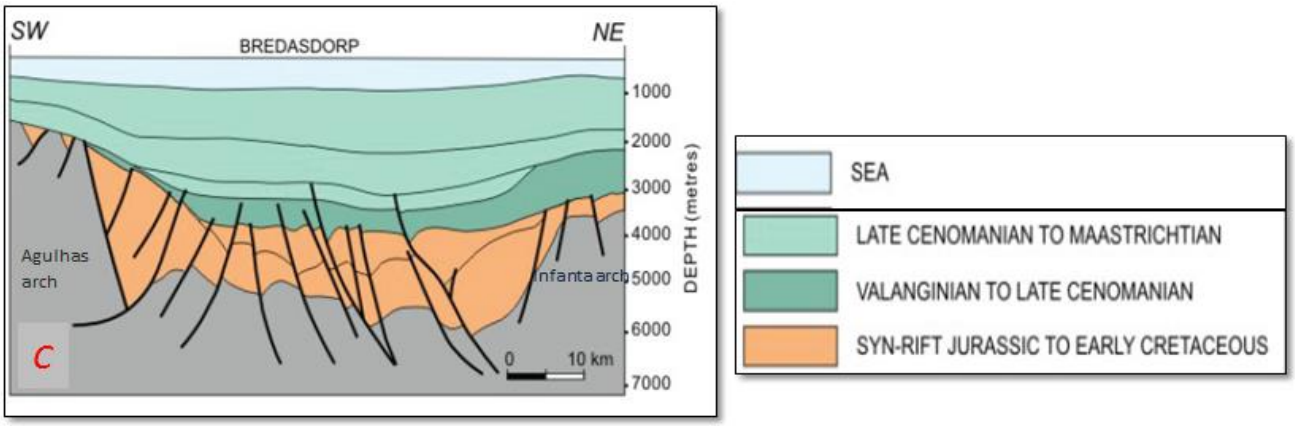

Figure 2.4. Rift faulting in the Bredasdorp Basin showing the bounding arches, the Agulhas arch on the SW and Infanta arch on the NE, (PASA , 2003).

Figure 2.2 shows the fault trends within the Bredasdorp Basin with the cross section in Figure 2.4 showing the normal faulting style between the bounding arches.
Sedimentation started at rifting onset in the Late Jurassic but the exact date is uncertain. Two phases of syn-rift sedimentation have been recognised by Jungslager (1996) within the Bredasdorp Basin with the Syn-rift I comprising of four lithogenetic units (listed below) as a response to major marine transgression and regression cycles.

1. The lower fluvial interval (LF) which represents the initial graben fill made of claystones, sandstones and conglomerates, deposited in alluvial fans and fluvial environments;
2. The lower shallow marine interval (SM) representing the first marine incursion into the basin, made of glauconitic fossiliferous sandstones;
3. The upper fluvial interval (UF) that comprises alluvial floodplain and meandering fluvial deposits;
4. The upper shallow marine interval (USM) made of massive glauconitic fossiliferous sandstones of Late-Valanginian age deposited as a transgressive beach facies.

Sediment supply during the rift phase was sourced from provenances in the northeast comprising of orthoquartzites and slates from the Cape Super group as well as sandstones and shales from the Karoo Super group (McMillan *et al.*, 1997).
The Syn-rift II succession was truncated by regional unconformity 1At1 which separates the shallow marine sediments from overlying deep-marine sediments. This truncation was triggered by upliftment of arches and horst blocks (Jungslager, 1996; Brown *et al*., 1995) and ceased syn-rift II sedimentation.

The onset of the deposits referred to as Syn-rift II (renewed rifting phase) is marked by the same 1At1 unconformity and refers to the sedimentary packages deposited in grabens and half grabens formed due to the initial transform movement on the AFFZ at about 121 Ma ago. This movement caused regional tectonism, it renewed block faulting, reactivated faults and caused local inversion (Jungslager, 1996). The overlying Syn-rift II interval contains

deep-water shales dated as Hauterivian (Broad et al, 2006) draping over titled fault blocks. Subsidence was rapid initially (~1At1/ Valanginian times) and diminished towards the end of the super cycle (5At1) (Brown *et al.,* 1995, McMillan *et al.,* 1997). Subsequently erosion occurred incising the 1At1 boundary via submarine valleys and canyons supplying /channelling sediments into the deeper parts of the Basin from northeast and southwest (McMillan *et al.,* 1997). The end of this phase of half-graben infill triggered by uplift is marked by the 6At1 unconformity (Brown *et al.,* 1995).

In Late-Hauterivian a transitional period occurred, where the margin changed from a passive margin to a transform margin. This change was influenced by tectonic events, eustatic sea level changes and probably by thermal subsidence and is characterised by repeated episodes of progradation and aggradation. It led to a deposition of basin-floor turbidites during the low-stands and organic rich shales during highstands (Jungslager., 1996). A fall in sea level followed during Early-Aptian to Mid-Albian, eroding material from the highstands forming stacked amalgamated channels and lobes (Turner et al., 2000).

The transition episode resulted in a drift phase which began in Mid-Albian and is marked by the 14At1 unconformity, by Late-Albian the Falkland Plateau had cleared the Columbine-Agulhas Arch and thermal subsidence became affective (Jungslager, 1996), this is associated with the deposition of deep-water basin-floor fans.

In the late Cenomanian minor warping and uplift occurred and is marked by the 15At1 unconformity (McMillan., 1997) and erosion is said to have been much intense in the eastern part of the Basin. Sands deposited at this time are the least significant as later basin-infill comprises of claystones and siltstones (Jungslager, 1996).

Overlying the 15At1 unconformity is a layer of shale rich with plankton and other organic materials associated with world-wide low-stand and basin starvation. At this time the South African plate had completely separated from the South American plate. In the Turonian, progradation occurred with a domal structure forming in the latest Cretaceous period (McMillan *et al.,* 1997).

The Tertiary to present day sedimentation is of high-stand shelf deposits comprising of glauconitic clays, which are biogenic clays with minor sands obtained from the erosion of the

Agulhas Arch flanks due to uplift in Late Cretaceous deposits which ended in Early Miocene. Unconformities in Holocene and late Pleistocene are found overlying the Miocene rocks. (McMillan *et al.*, 1997).

All the above mentioned features can be seen on Figure 2.5, which is a generalised chronostratigraphy of the Bredasdorp Basin based on the results of sequence stratigraphy studies (after Brown *et al.*, 1996; Jungslager, 1996 ; Soekor, 1994a,b).

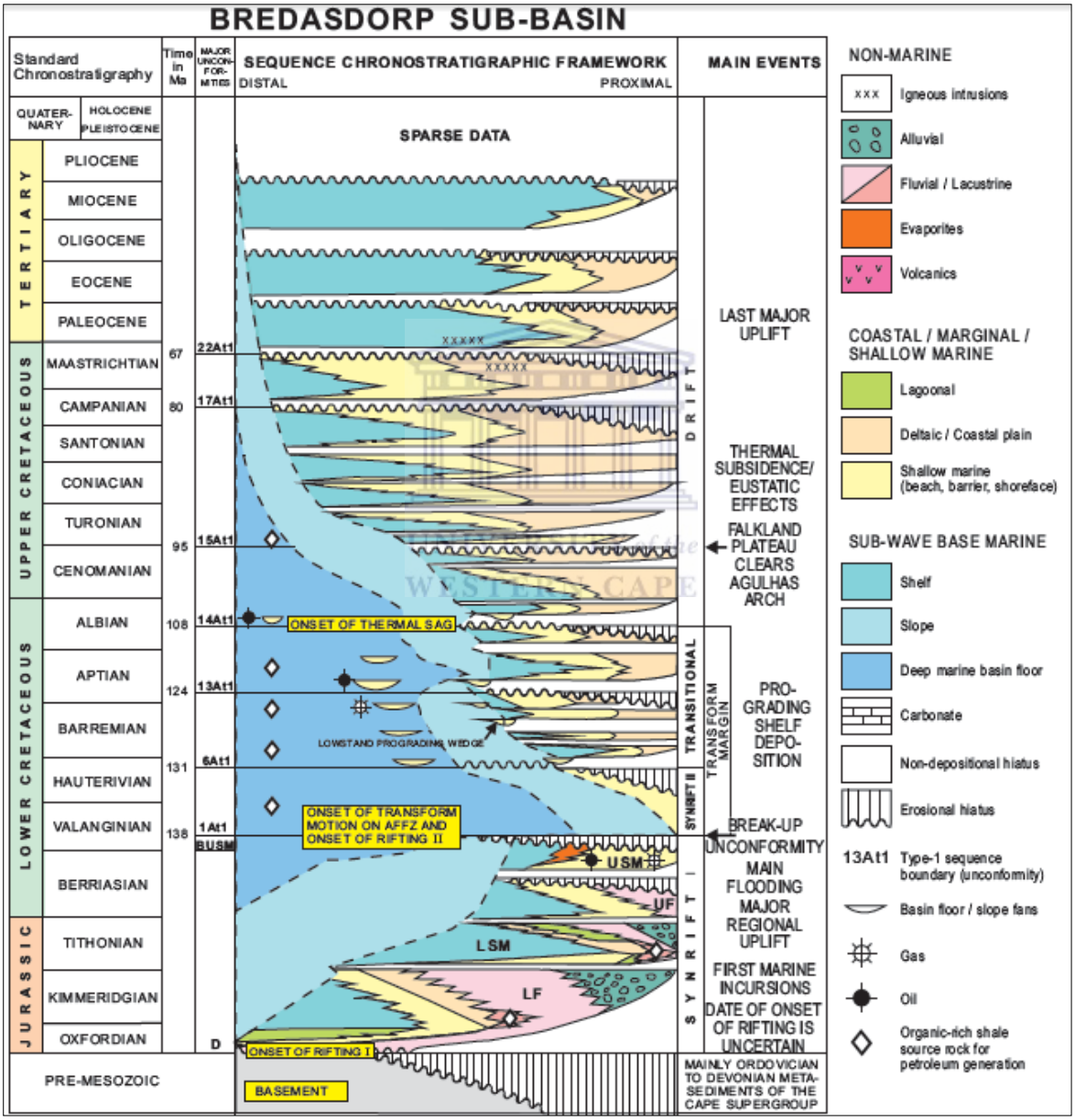

Figure 2.5. Chronostratigraphy of the Bredasdorp sub-basin, (Petroleum Agency of South Africa, 2003).

*No vertical/horizontal scale or thickness is implied on figure 2.5.

CHAPTER 3

METHODOLOGY

The methodology used for seismic interpretation and restoration follows the workflow designated by Move© shown in the flowchart below where seismic images were imported into the software as SEGY data files (which is a standard format for geo-physical seismic data) and interpreted by "picking faults, horizons and markers". The interpreted section was depth converted using a defined depth-time function calculated from check-shot data and quality controlled using horizon markers. Sequential restoration and decompaction were performed as a step-wise process to test the proposed solution.

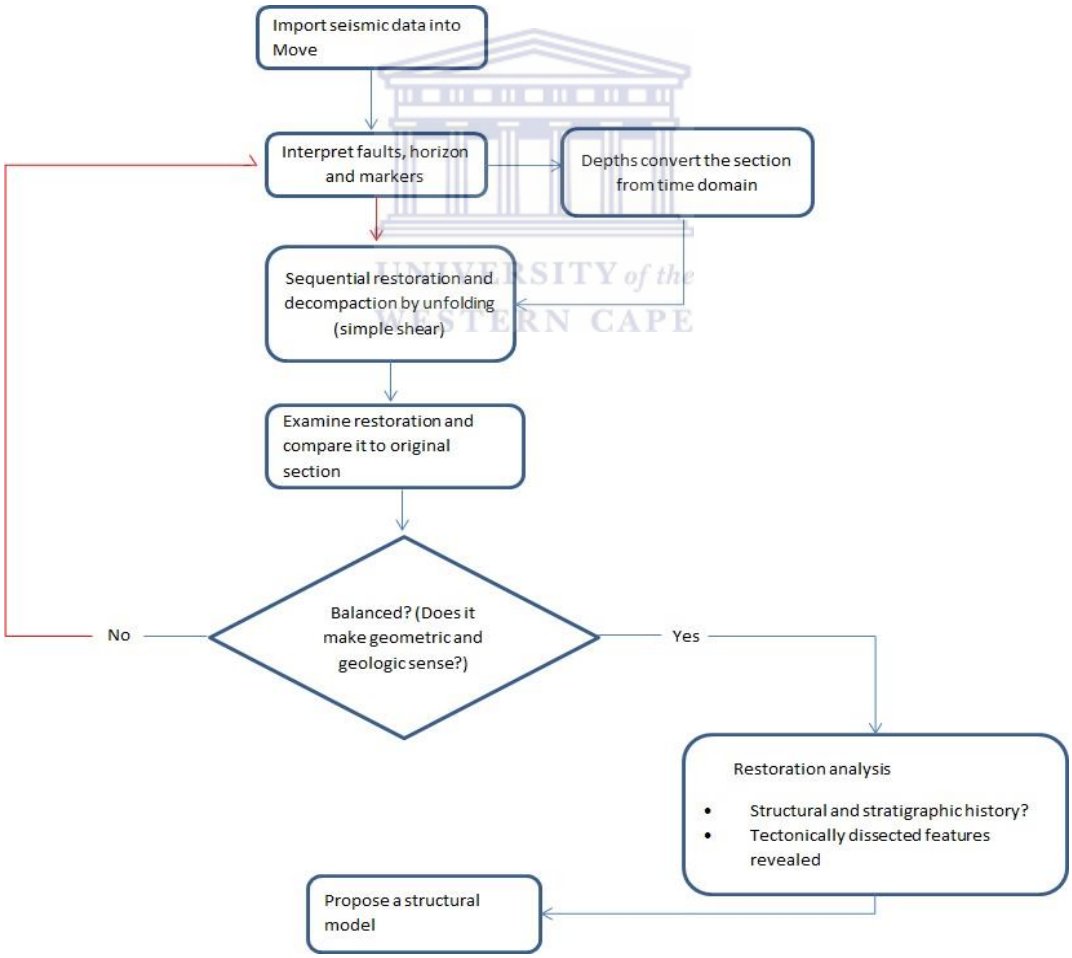

Figure 3.1 Seismic interpretation and restoration workflow.

SEISMIC INTERPRETATION

Faults were interpreted in each section at points where seismic reflectors terminate and horizons picked along continuous reflectors were interrupted. Correlations of horizons across some faulted blocks are somewhat of an uncertainty as the seismic reflectors are poorly visible (chaotic) but with an understating of the stress regime an interactive structural modelling tool was used to construct the horizons and predict the expected fault behaviour at depth. To lower the degree of uncertainty analogues from experiments, geological models and geological examples were also used as reference tools to aid the interpretation. Horizon markers provided information on the different depositional units interpreted.

DEPTH CONVERSION

Depth conversion is an important and delicate step in seismic interpretation workflow as seismic data vertical scale is in time domain (Two-Way-Travel time). To have an accurate geological interpretation of the subsurface structures, seismic imagery needs to be in depth domain.

Depth was approximated by defining a depth-time curve from scatter plots, other conversion methods were limited by well data because velocities of deeper lying strata are unavailable as wells only penetrate to a certain depth. With the use of check-shot data (a type of borehole seismic data designed to measure the seismic travel time from the surface to a known depth) from a well closest to the seismic survey a depth versus time relationship was established as a function which best honours the relationship between time and depth domains.

By defining the function type (Time/Depth, Depth/Time etc.), the equation type (linear, quadratic etc.), the parameter defining the equation and the units used to define the equation the conversion was simply calculated in Move©. Horizon markers were loaded to validate the conversion where depth was certain.

DECOMPACTION

Compaction is defined as a process by which sediments progressively lose porosity due to gravitational loading by overlying strata resulting in volumetric dimension change. Primarily, sediments have an open framework of particles and pore spaces filled with water, but with continued deposition porosity of the underlying strata becomes less as the particle-to-particle stress increases.

To better understand the paleo-geometry it is thus necessary to move the layers up the depth-porosity curve which is simply removing the overlying depositional layers and its effects on underlying layers. A more detailed workflow is explained in Chapter 4 with the formulas used and parameters.

SECTION RESTORATION

The interpreted seismic section is then restored which is a technique used to reverse the effects of deformation as a structural interpretation validation tool .This process also provides insight of the paleo-architecture of the basin.

Several algorithms (Table 3.1) are available for the restoration process and the recommendation on which to use is dependent on the structural style observed or interpreted on the section which is a result of the type of deformation undergone by a body of rock. The deformation algorithms are estimations and idealisms of original strain paths and stray from reality (Ramsey and Huber, 1987). Selection of the appropriate algorithm is crucial for proper restoration.

Restoration algorithm	Deformation mechanism	Advantages and limitations
1.Vertical/simple shear	A slip on closely spaced planes oblique with shear strain oblique to bedding	It gives a more accurate approximation to the behavior of rocks under extension tectonics as it preserves area, however fails to preserve bed length and thickness.
2. Flexural slip	The slip between layers is visible on observation scale	Preserves both area and line length and used for fold & thrust belts, inversion structures and in areas of salt tectonics. This algorithm fails to preserve thickness.
3.Line length	Only holds valid for rigid body displacement which may include translation and rotation	Assumes all line lengths and thicknesses are consistent during deformation and is used to quantify tectonic shorting and or extension through time.

Table.3.1 a list of restoration algorithms

A simple shear unfolding algorithm was used in this study as a recommendation of the best approximation in restoration of extensional tectonic regime where there is a combination of antithetic and synthetic faulting (Yamada and McClay, 2003).

CHAPTER 4

RESULTS AND DISCUSSION

SEISMIC TIME TO DEPTH CONVERSION

The methodology to depth convert the seismic sections is discussed in chapter 3, using check-shot data from wells outlined in column 2 of Table 4.1 for each respective section. The scatter plots yielded polynomial relation trends by observing the best line of fit where the regression value is ~1, which is best described by the equation:

$$y = ax^2+bx+c$$

y is the true vertical depth in meters (m)

x is the two-way-time in millisecond (ms)

a, b and c are known values (coefficients)

Table 4.1 Shows the quadratic equation yielded from the check shot data.

SEISMIC SECTION	WELL NUMBER	DEPTH-TIME RELATION
Line_XL_479	F-A 6	Quadratic (polynomial) trend $y = 0.0003x^2+0.651x+64.541$ $R^2= 9.93$
Line_XL_1248	F-AR5	Quadratic (polynomial) trend $y = 0.0003x^2+0.7715x+22.006$ $R^2= 9.89$
Line_XL_946	F-A 10	Quadratic (polynomial) trend $y = 0.0003x^2+0.7314x+61.94$ $R^2= 9.87$
Line_XL_1687	F-AH5	Quadratic (polynomial) trend $y = 0.0003x^2+0.8909x+123.31$ $R^2= 9.96$

DEPTH TIME CURVES

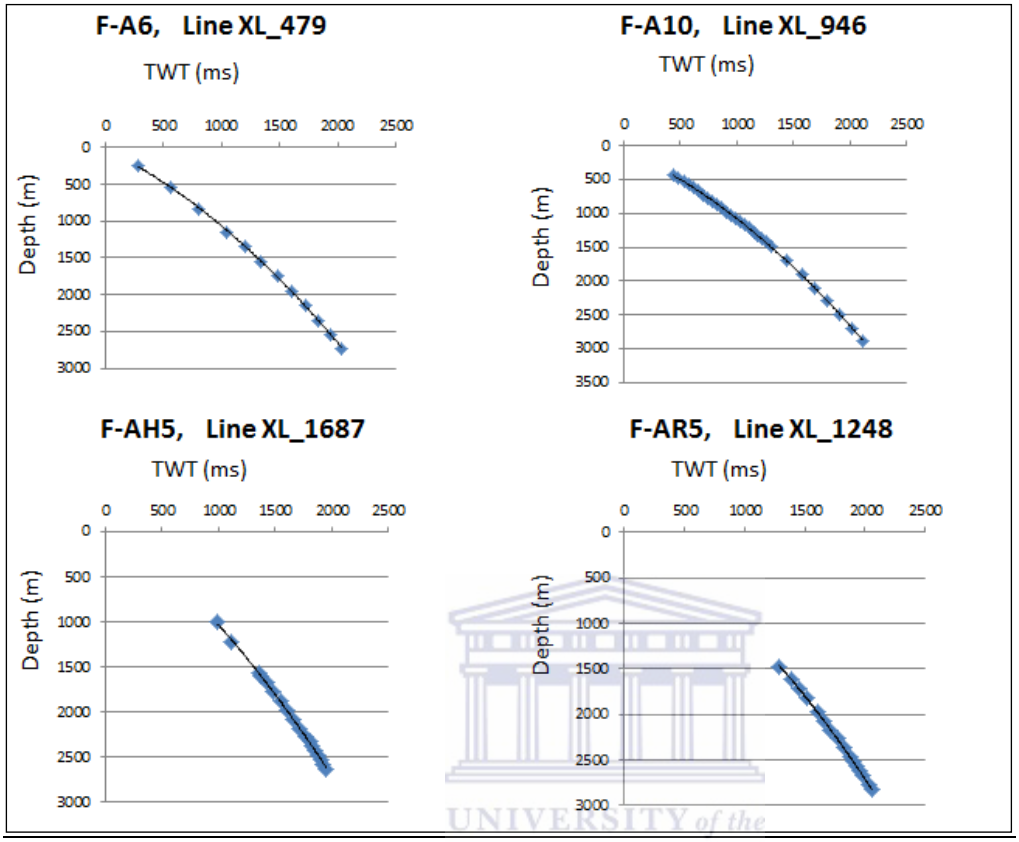

Figure 4.1. Scatter plots of check-shot data used to derive depth vs time curves.

Check-shot data is spatial and was not measured at constant depths in all the wells hence some of the scatter plots show a high concentration of dots than others.

*Comments: The equations used remain true and valid up to a certain depth (honouring well data). At deeper depths, where no velocity data was available, regression analysis was used to model expected values of Two-Way-Time. Indicated on the plots is the best line of fit approximated by using the highest regression value.

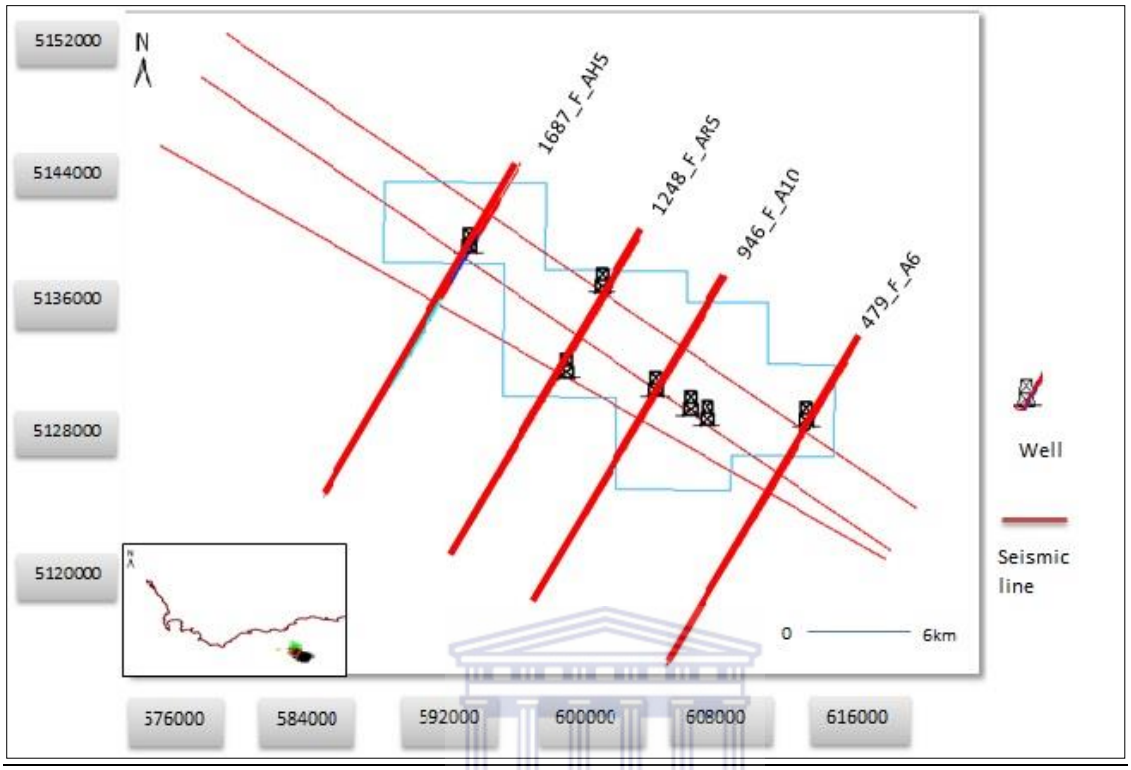

Figure 4 .2 Study area seismic lines of F-A gas field in Block 9, the strike lines are NW-SE trending while dip line trend NE-SW.

The area under study is highly dominated by faults striking in the NW-SE direction with two opposite dips showing normal kinematics. The set of faults more at the south-westerly end dip towards north east while the set at the north-easterly end dips to the south west defining a symmetric geometry, also known as a *graben* (Figure 4.3).

The interpreted horizons (orange, maroon and pink) in Figure 4.1 correspond to the upper fluvial and upper shallow marine depositional units respectively; this was extrapolated from well-horizon markers. The light purple was interpreted using a construction tool provided by Move© and the rift onset horizon was interpreted as shown in Figure 4.4 as there are no wells intersecting the older depositional units.

Line_XL_1248

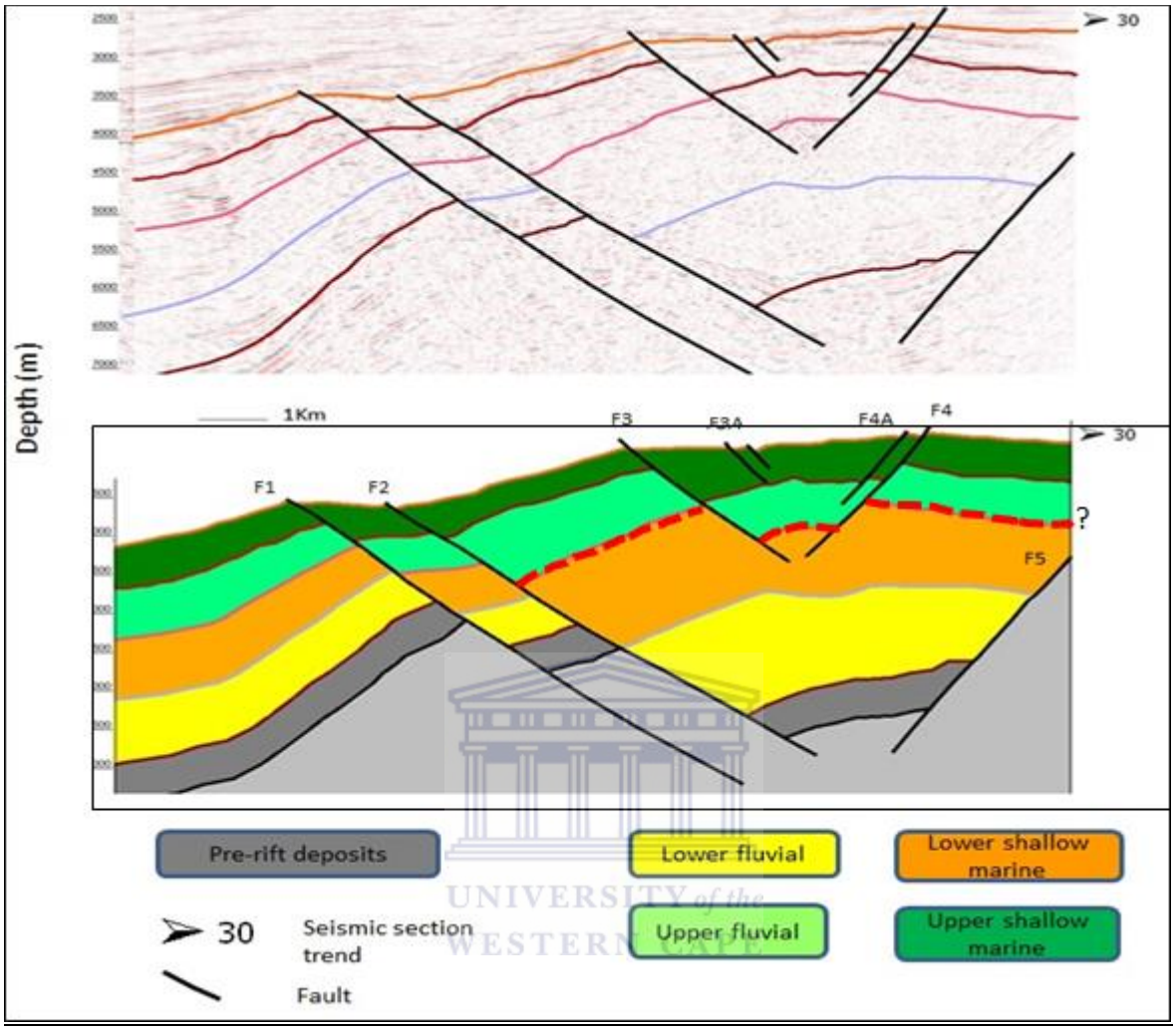

Figure 4.3. Depth converted section line XL-1248 interpretation.

Faults F1, F2 and F3 dip towards the NE whilst F4 and F5 dip to the SW forming a conjugate set with dip angles less than 40 degrees and are categorised as low-angle normal faults. The dips of faults F1 to F4 display angles consistent with listric geometry in that with increasing depth the angle of dip decreases resulting in a shape slightly concave upward.In contrast F5 is more planar in shape showing a constant dip with increasing depth leading to classification as a normal fault.

Dip angle values are tabulated in Table 4.2 measured along the fault trajectory assuming that the seismic section is parallel to the direction of dip.

*an un-interpreted seismic section line 1248 can be viewed in Appendix A, page 53.

Table 4.2. Measured dip angle values along the fault trajectory with increasing depth.

FAULT	INTERVAL OF MESUREMENT	DIP ANGLE
F1	3500-4506 6000-7000	25.7 19.3
F2	3503-4506 6000-6664	22.5 19.2
F3	2740-3402 3463-4185	26.2 24
F4	2519-3192 3213-4125	39.9 32
F5	4235-5209 5350-6634	36 36.3

The displacement on the fault is not constant over the fault surface, the distance decreases up the syn-rift package. Maximum heave and throw are measured across the youngest pre-rift package Figure 4.4 shows the measured displacement along F1 trajectory with tabulated results in Table 4.3.

*An assumption that the section line is parallel to the direction of dip had to be made for angle measurements.

*The seismic section trend is 030^{o} for all the displayed captions (Figure 4.4 - 4.8).

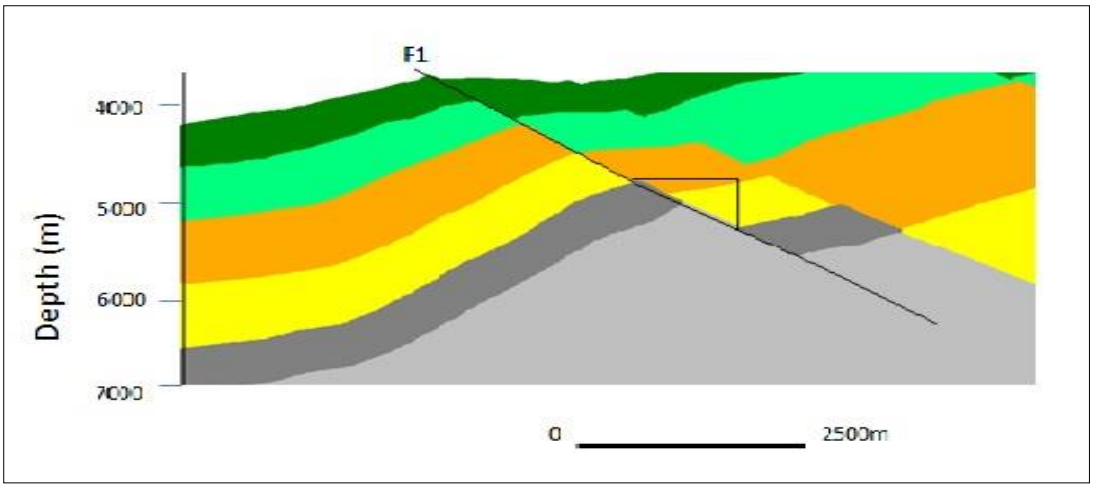

Figure 4.4. Heave and Throw measured along Fault 1

Table 4.3 shows calculated heave and throw across F1

Horizon markers	Heave and throw (m)	Displacement (m)
Grey horizon	H = 1429,96 V = 528,86	1544,19
Yellow horizon	H = 1227,90 V = 536,23	1339,88
Orange horizon	H = 746,06 V = 373,03	834,13
Light green horizon	H = 528,46 V = 233,15	577,61
Dark green horizon	H = 13,89 V = 77,72	160,03

The pre-rift sequence is recognised by having parallel to sub-parallel seismic reflectors with constant strata thickness and seismic facies that can be traced across the faults. The commencement of rifting is shown by onlapping sequences on the downthrown fault block exhibiting a wedge-like geometry with hummocky seismic facies (Figure 4.4).

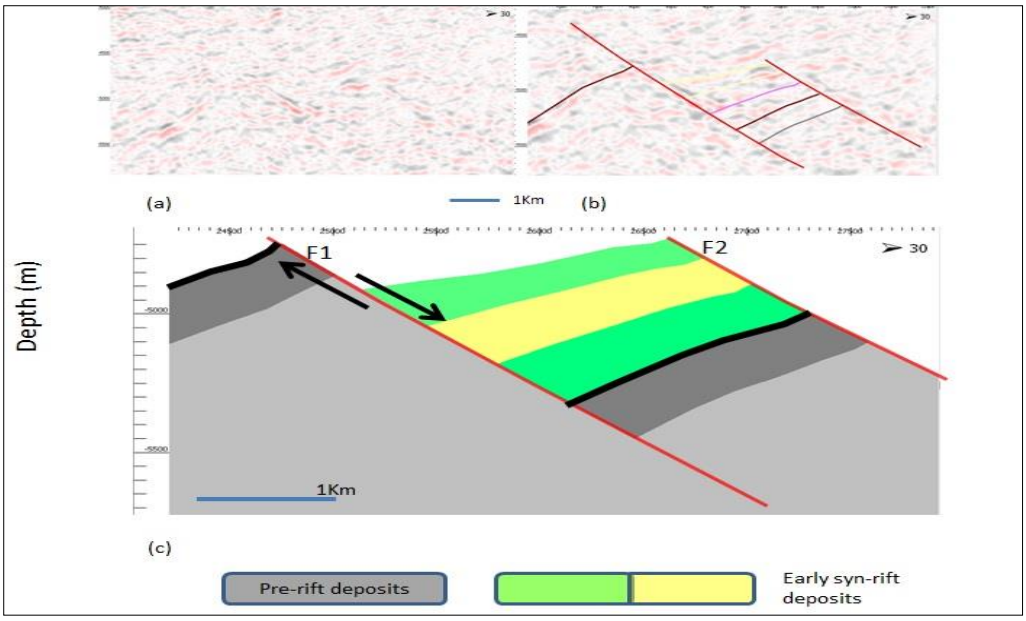

Figure 4.5 (a) seismic section showing rift-onset (b) interpretation of rift onset unconformity and (c) shows a schematic section from the interpretation.

Syn-rift deposits thicken towards the active fault as the seismic reflectors diverge and converge away from the fault boundary. The rift onset unconformity is correlated across the series of normal faults shown in Figure 4.5 in interpreting the distribution of syn-rift deposits.

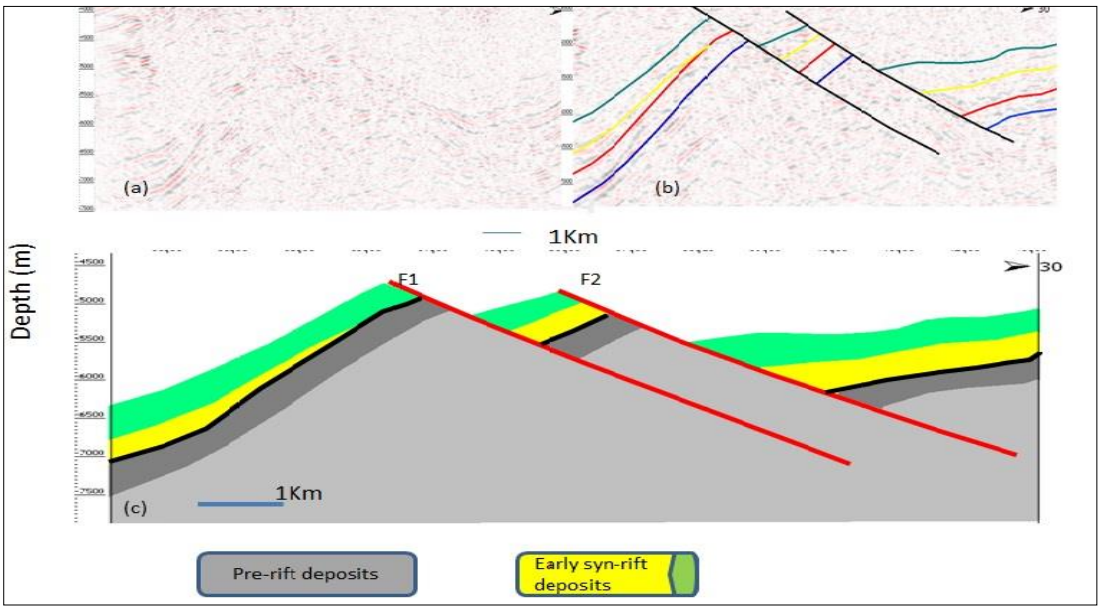

Figure 4.6 (a) and (b) Seismic section showing the correlated rift on-set unconformity and early syn-rift deposits. (c) Shows a schematic section.

The end of the rifting is marked by an unconformity which is erosional and angular in some areas. The post-rift sediments onlap the syn-rift deposits, this is shown by sub-parallel reflectors in earlier deposited package to parallel with much younger deposits (Figure 4.6).

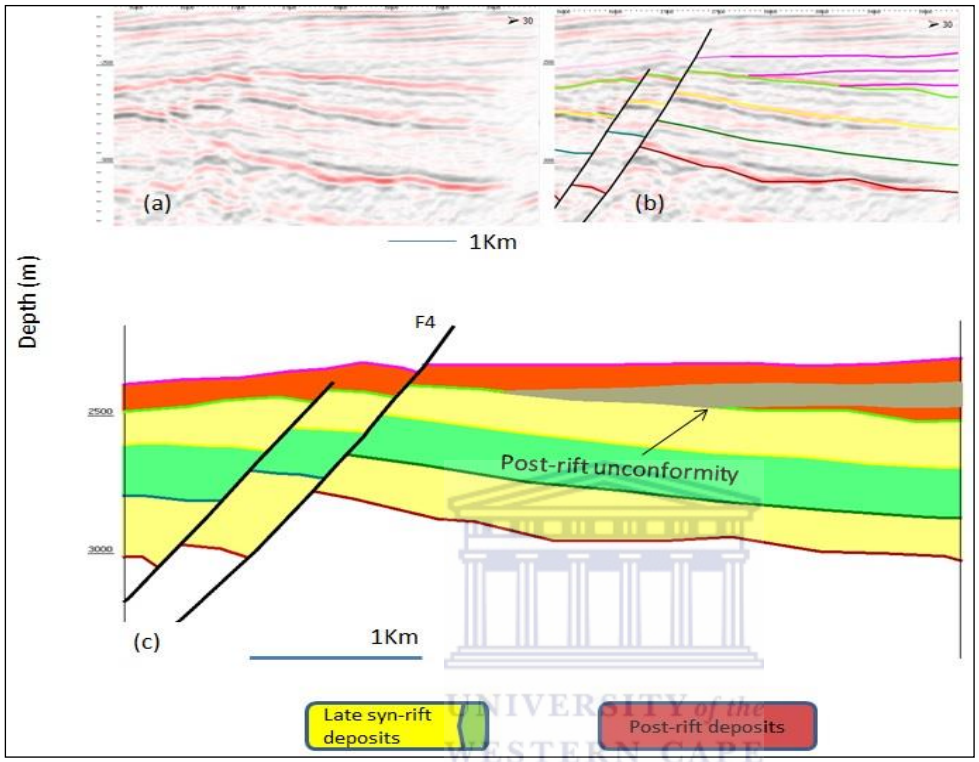

Figure 4.7(a) and (b) shows interpretation of the end of rifting marked by an unconformity and (c) is the schematic section

The early post-rift and late syn-rift sequence show evidence of inversion which is more localized, there is an upliftment above the regional elevation (assumable) with the hanging wall anticlines forming a harpoon structure (Figure 4.7).

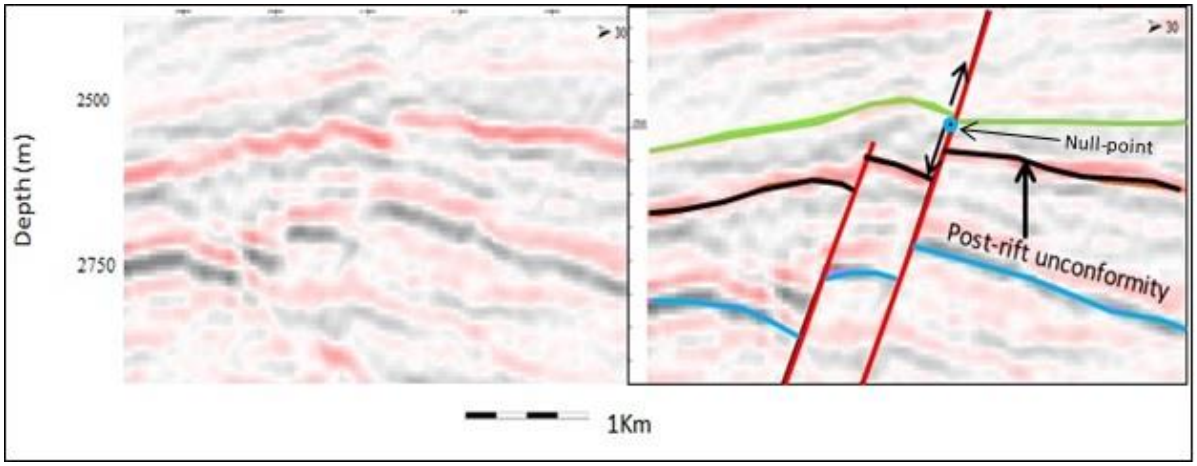

Figure 4.8. Showing inversion tectonics interpreted just above the post rift unconformity along F4.

Seismic lines XL_479, XL_1687 and XL_946 were also interpreted in a similar fashion as XL_1248 interpreted above and yielded similar results. Faults F1-F5 are laterally continuous and are seen in all of the above sections having a listric geometry (Table 4.4) with a displacement that is inconsistent with depth and decreases up the section.

The three deposition generations were also interpreted and identified from these sections which are 1). The pre-rift sequence 2). Syn-rift sequence and 3) the post-rift sequence displaying similar characteristics as seen in section XL_1248 with thickening syn-rift strata and almost uniform thickness with pre-rift and post-rift strata (Figures 4.7 - 4.10)

Table 4.4. Measured dip along the fault trajectory

Section profile	XL_479		XL_1687		XL_946	
Fault	Interval	Angle	Interval	Angle	Interval	Angle
F1	3541-4884 6000-7308	33.8 30.2	3532-4767 5906-6561	29.9 23.9	3539-4750 5669-6952	31 28
F2	2861-4623 5250-6942	30.6 30.1	3393-4475 5500-6416	27.9 24.5	3059-4197 5094-6399	26 25.1
F3	2669-3541 3663-4483	28.2 37.7	3165-3690 3774-4322	20.8 25	2756-3550 3700-4353	25.5 21.9
F4	2599-3489 3646-4500	38.7 40	2959-3538 3668-4315	36.2 37.7	2808-3414 3508-4155	42 34.6
F5	5355-6890	39	3523-4650 5221-6295	35.4 34.1	4406-5334 5470-6399	32.2 31.5

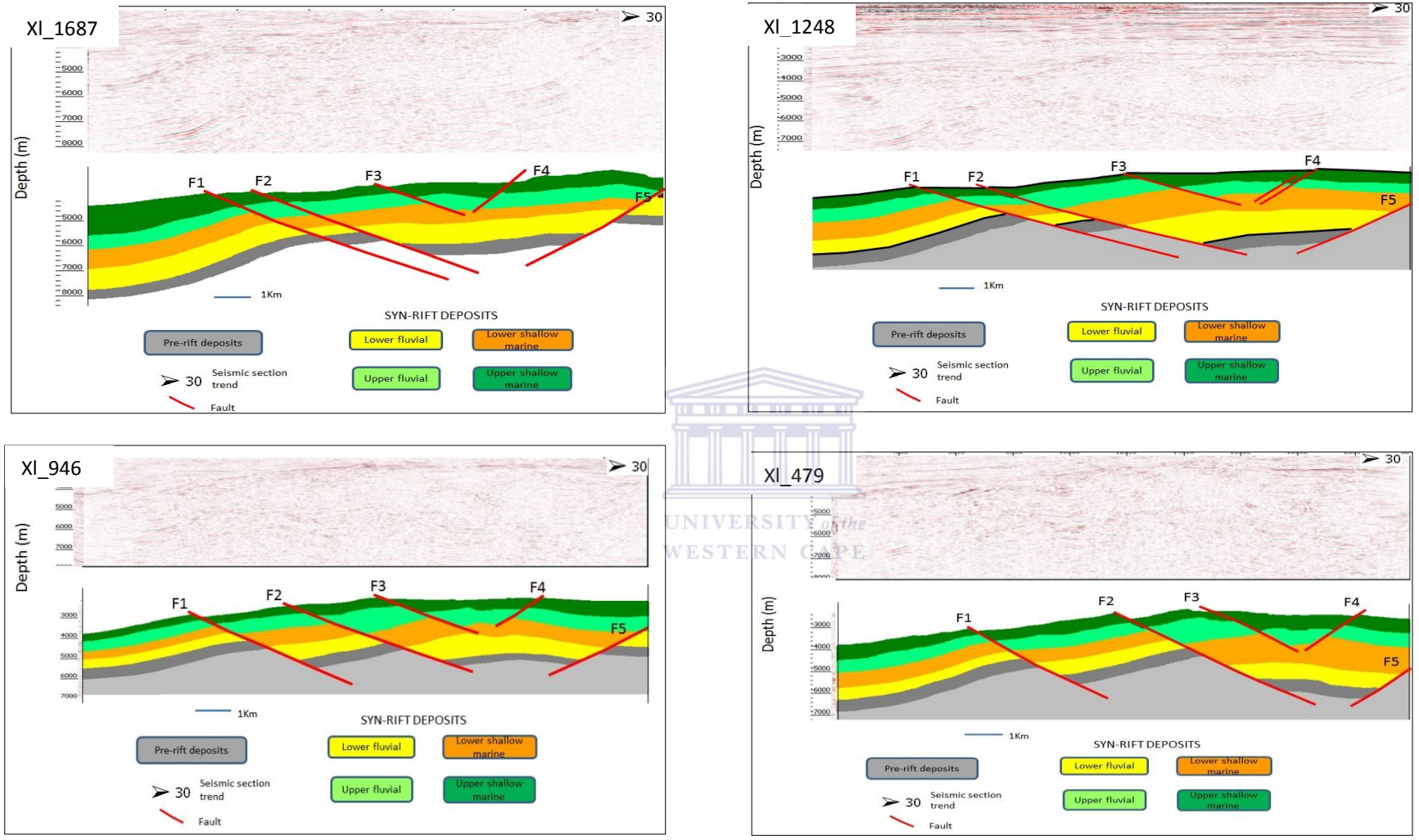

Figures 4.9 - 4.12. Seismic section interpretation.

RESTORATION RESULTS

Structural restoration was achieved using the sequential restoration workflow outlined in Chapter 3 which and a restoration algorithm that is dependent on the observed deformational style which in this case is a simple shear environment. The seismic image was firstly flattened in an attempt of removing compaction formed by drift related deposits to reveal the paleogeometry of the underlying structures. Faults were than restored by matching the hanging wall and footwall cut-offs, this was a step-by-step process of moving-up the downthrown faulted block to its initial position prior to displacement and restore it to its assumable paleo depositional slope. Decompaction followed restoration as a sequential repetitive process with every depositional layer removed.

The restoration results of the geological sections are shown in Figures 4.11- 4.14 . Total extension, average extension and extensional rates at different times are listed in Table 4.9-4.13, while the plot of extensional ratios versus time is shown in Figure 4.15. The ages of the interpreted faults are in Table 4.8.

DECOMPACTION

Allen A.P and Allen J.R (2005) explain compaction as a change in dimension of a volume of sediments as a result of gravitational load of an overlying column of water-saturated sediment load. This gravitational loading results in porosity reduction due to volumetric strain which consequently decreases the stratigraphic thickness.

Empirical studies conducted by Slater and Christie (1980) show that porosity decreases exponentially with depth and in general the relationship is described by equation (1) which is the function used in Move© for decompacting.

$$Ø = Ø_0 e^{-cy} \quad (1)$$

Where Ø : the porosity at the investigated depth

$Ø_0$: the surface porosity (porosity at deposition)

C : rock specific compaction constant y: the depth

Table 4.5. Standard compaction and surface porosity values determined by Slater and Christie (1980) for different lithologies.

Lithology	Surface porosity (%)	Compaction factor ($Km^{-1)}$
sandstone	0.49	0.27
shale	0.63	0.51
Shaley-sandstone	0.56	0.39

Table 1.1 shows standard compaction values for pure sandstone, shale and shaley-sand stone and it cannot be used for this exercise as the depositional units being studied possible have quantities of different lithologies thus a more detailed lithological description was done using the standard velocity vs density curve by Birch (1961) Figure 1.1..

The velocity was calculated by converting two-way-time (milliseconds) to one-way-time (seconds) of the 4 depositional units intervals which are: Upper shallow marine (USM), upper fluvial (UF), lower shallow marine (LSM) and lower fluvial (LF) interval interpreted from the seismic sections.

Table 4.6. Depth intervals of different depositional units with the measured two-way-two (ms) and velocities.

Depositional units	Depth (investigation zone)	TWT (ms)	One way time (s)	Velocity (m/s)
USM	2703-3208	2072-2329	1,036-1,165	3899
UF	3208-3734	2329-2576	1,165-1,288	4293
LSM	3734-4576	2576-2942	1,288-1,421	4601.09
LF	4576-5692	2942-3400	1,421-1,700	4894

Velocity calculations:

$$V = \Delta \text{ depth} / \Delta \text{ time} \quad (2)$$

Where Δ depth is the investigation depth interval

Δ time is the one-way-time difference in the investigation interval

Density values for the different units were calculated using Gardner's equation

$$\rho = \alpha V^{(\beta)} \quad (3)$$

ρ: bulk density of the lithology

V: P-wave velocity (m/s)

α and β are empirically derived constant which are respectively 0.31 and 0.25

Table 4 7. Calculated velocity and density values with corresponding lithological description.

Depositional units	Velocity (m/s)	Density (g/cc or g/cm^3)	Lithological description (Sandstone: Shale) ratio	Compaction factor (Km^{-1})
USM	3899	2.44	70:30	0.342
UF	4293	2.509	60:40	0.366
LSM	4601.09	2.58	50:50	0.39
LF	4894	2.592	30:70	0.438

*The compaction factor is calculated as follows

Compaction factor = ((sandstone ratio*0.27) + (shale ratio*0.51))

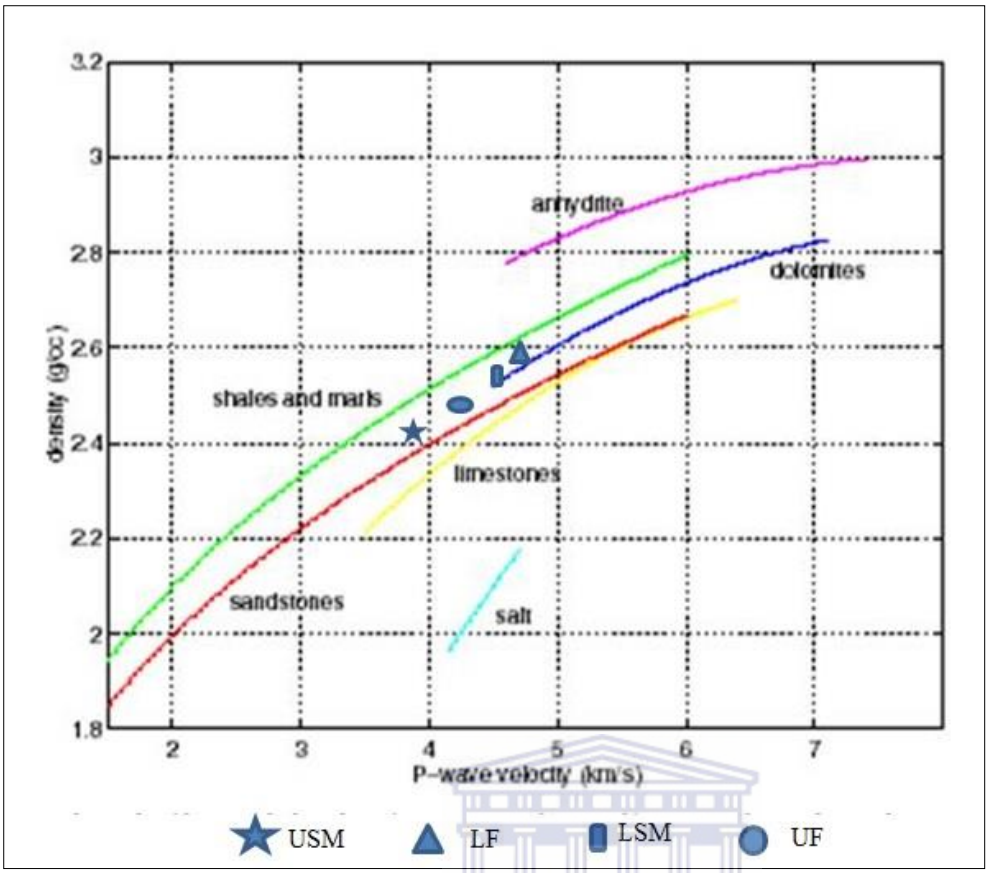

Figure 4.13. Lithological classification curves using P-wave velocity and density of the material after Birch (1961).

*Fault labelling in the restored section profile (Figure 4.11 - 4.14) is the similar to figures 4.7-4.10.

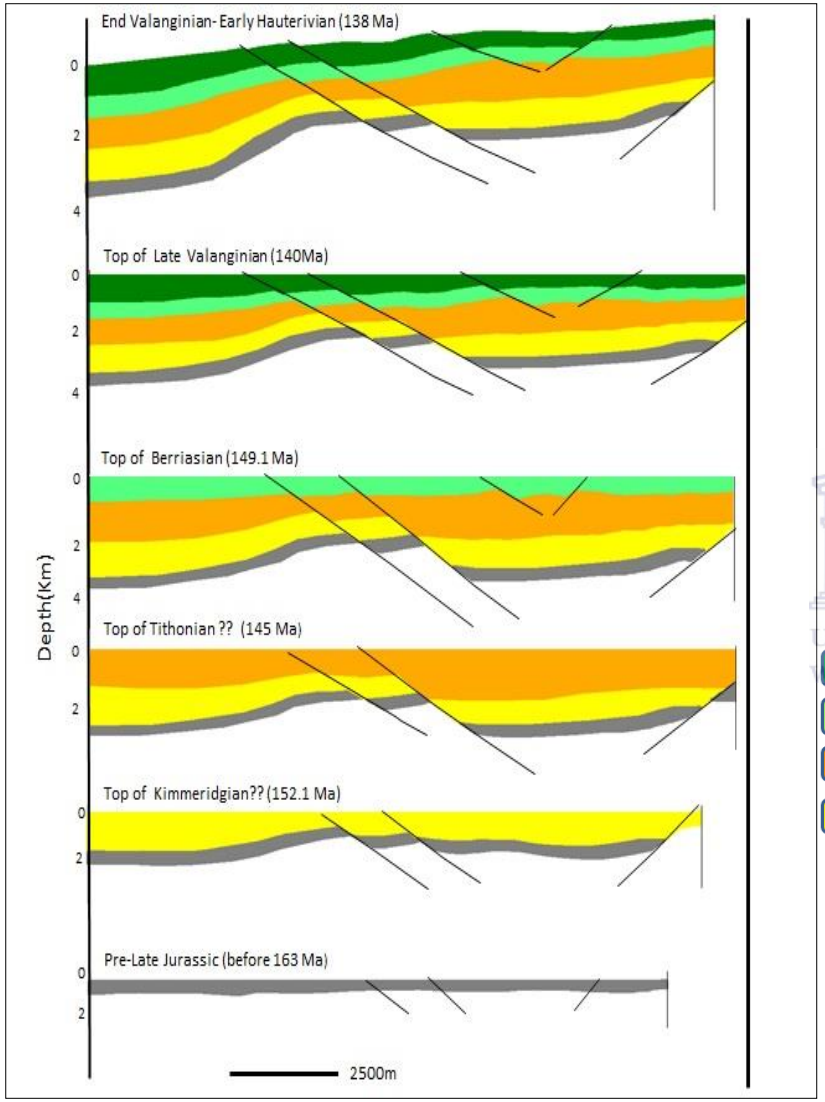

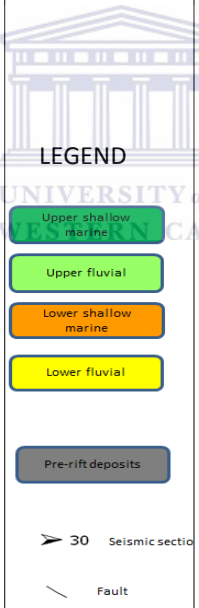

Figure 4.14. Restored section line 1687.

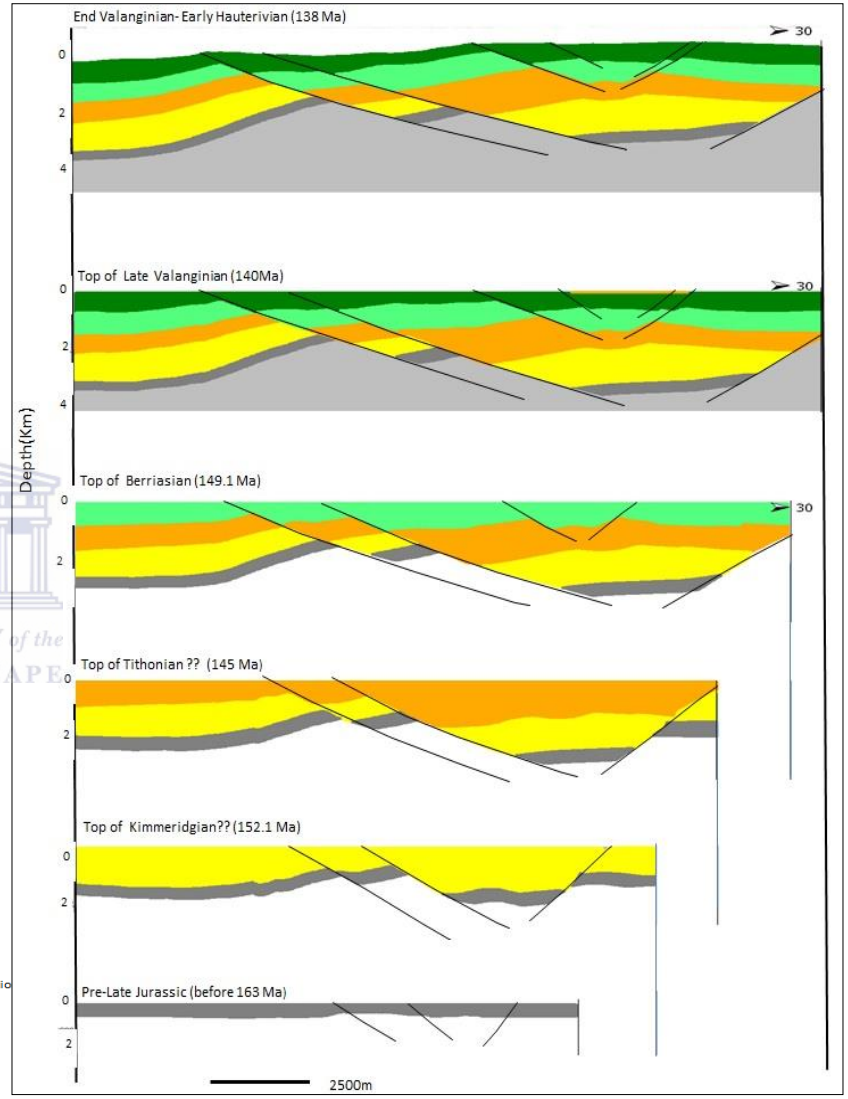

Figure 4.15. Restored section line 1248.

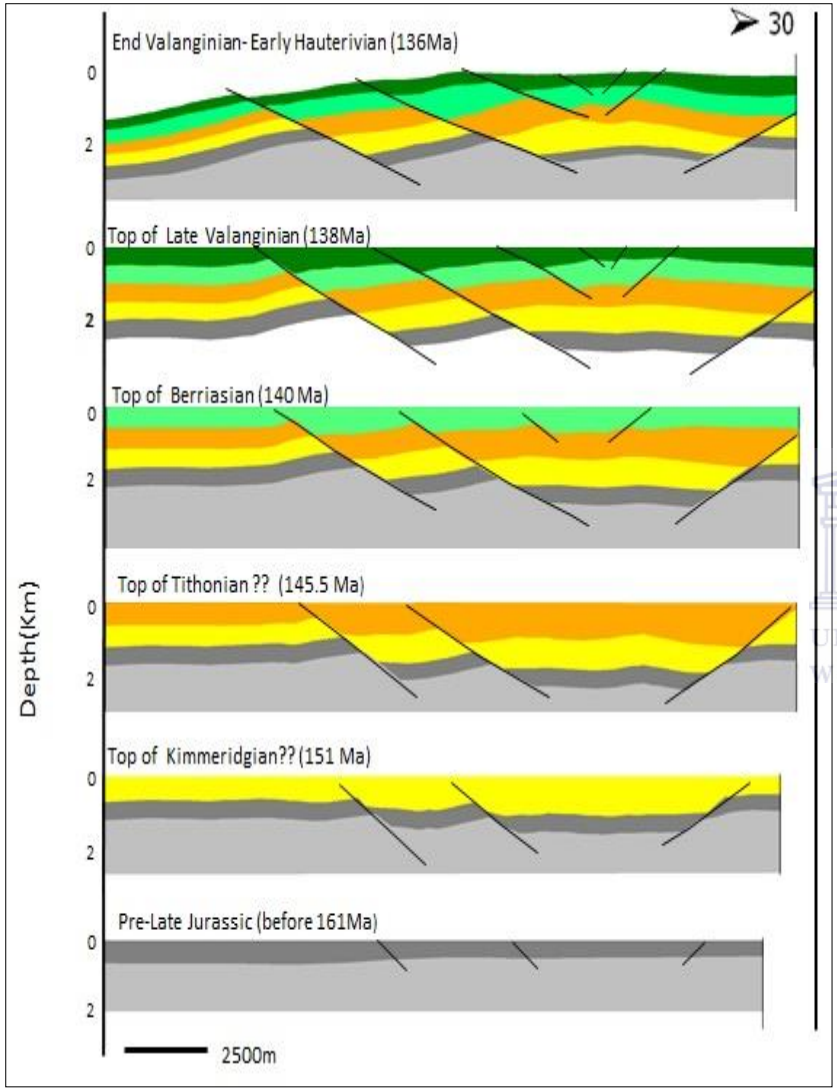

Figure 4.16 Restored section line 946.

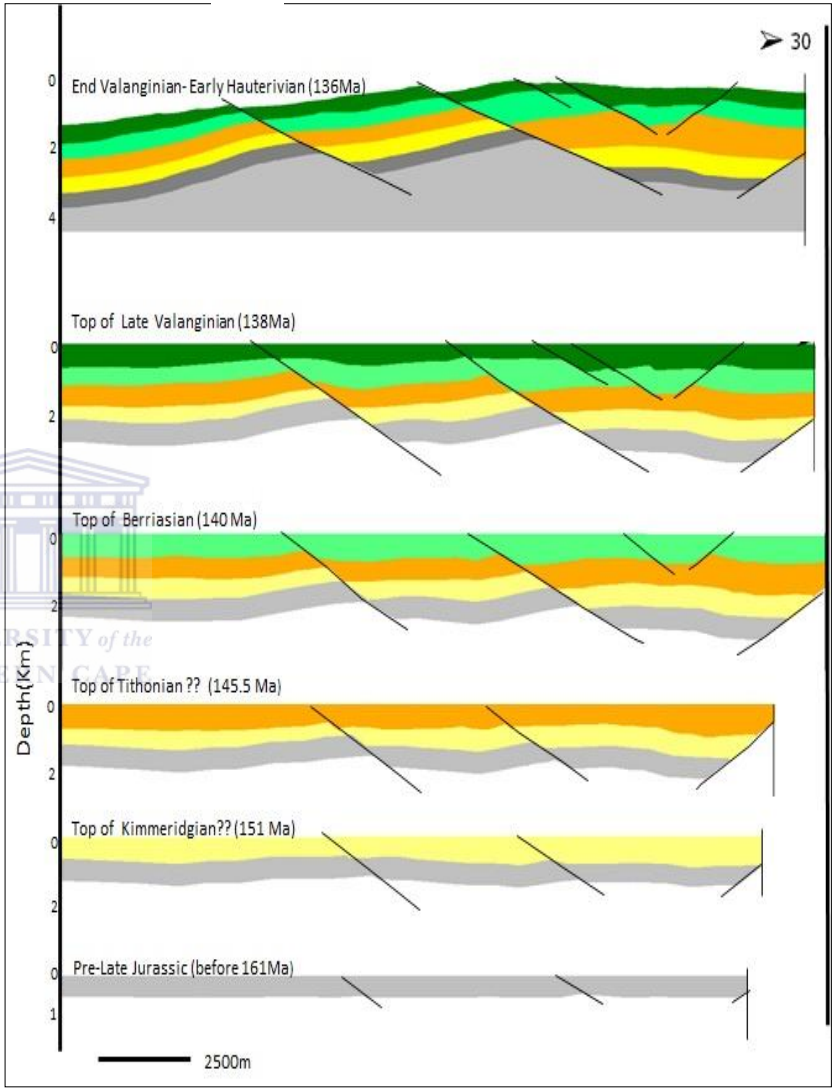

Figure 4.17 Restored section line 479.

Table 4.8 Fault ages attained from section restoration (all four seismic sections).

Period in time (Ma)	Fault 1	Fault 2	Fault 3	Fault 3a	Fault 4a	Fault 4	Fault 5
Pre-Late Jurassic (before 163 Ma)	present	present	absent	absent	absent	absent	present
End Kimmeridgian (~151Ma)	present	present	absent	absent	absent	absent	present
End Tithonian (~145.5 Ma)	present	present	absent	absent	absent	absent	present
End Berriasian (~140 Ma)	present	present	Present	absent	absent	present	Out of seismic scope
Late Valanginian (~138 Ma)	present	present	Present	absent	absent	present	Out of seismic scope
End Valanginian-Early Hauterivian (~136)	present	present	present	Present	present	present	Out of seismic scope

Table 4.9. Extensional results for section 1687

Period in time (Ma)	Initial length (m)	Extension amount (m)	Extension ratio (%)	Cum. Ext^{n}. Ratio (%)	Average Ext^{n}. rate (mm/yr)
Pre-Late Jurassic (before 163 Ma)	13812	----------	----------	----------	
End Kimmeridgian (~151Ma)	14661.9	849.9	6.15	6.15	0.08
End Tithonian (~145.5 Ma)	15474.1	812.2	5.54	12.03	0.14
End Berriasian (~140 Ma)	15385.5	-88.6 (compression?)	-0.5	11.4	--0.016
Late Valanginian (~138 Ma)	15654.7	269.2	1.74	13.34	0.135
End Valanginian-Early Hauterivian (~136)	14830	-824.7 (compression?)	-5.3	7.37	-0.412
	----------	Total Ext^{n}. = 1018	= 7.37	= 7.37	

Table 4.10. Extensional results for section 1248

Period in time (Ma)	Initial length (m)	Extension amount (m)	Extension ratio (%)	Cumulative Ext^{n} ratio (%)	Average ext^{n}. Rate (mm/yr)
Pre-Late Jurassic (before 161 Ma)	12288.8	----------	----------	----------	---------
End Kimmeridgian (~151 Ma)	14173.6	1884.8	15.3	15.3	0.1884
End Tithonian (~145.5 Ma)	15669.3	1495.7	10.5	27	0.271
End Berriasian (~140 Ma)	17472.7	1803.4	11.5	42	0.33
Late Valanginian (~138 Ma)	18234.6	761.9	4.4	48.4	0.38
End Valanginian-Early Hauterivian (~136 Ma)	18234.6	0	0	48.4	0
total ext^{n}.	--------	= 5945.8	= 48.4	= 48.4	

Table 4.11. Extensional results for section 946

Period in time (Ma)	Initial length (m)	Extension amount (m)	Extension ratio (%)	Cum. Ext^{n}. Ratio (%)	Average Ext^{n}. rate (mm/yr)
Pre-Late Jurassic (before 163 Ma)	17377.2	----------	----------	----------	--------
End Kimmeridgian (~151Ma)	18315.5	938.3	5.4	5.4	0.09
End Tithonian (~145.5 Ma)	19424.1	1108.6	6.05	11.8	0.2
End Berriasian (~140 Ma)	19711.5	287.4	1.47	13.4	0.05
Late Valanginian (~138 Ma)	20508.5	797	4.04	18.01	0.4
End Valanginian-Early Hauterivian (~136)	20117.5	-391	-1.93	15.8	-0.2
	----------	Total Ext^{n}. = 2743.9	= 15.8	= 15.8	

Table 4.12. Extensional results for section 479

Period in time (Ma)	Initial length (m)	Extension amount (m)	Extension ratio (%)	Cum. Ext^{n}. Ratio (%)	Average Ext^{n}. rate (mm/yr)
Pre-Late Jurassic (before 161 Ma)	19935.5	----------	----------	----------	
End Kimmeridgian (~151Ma)	20771.1	835.6	4.2	4.2	0.083
End Tithonian (~145.5 Ma)	20182.4	-588.7	-2.8	1.23	-0.1
End Berriasian (~140 Ma)	21019.8	837.4	4.1	5.4	0.15
Late Valanginian (~138 Ma)	20858.7	-161.1	-0.7	4.63	-0.08
End Valanginian-Early Hauterivian (~136)	20750.2	-108.5	-0.5	4.08	-0.054
	----------	Total Ext^{n}. = 832.7	= 4.08	= 4.08	

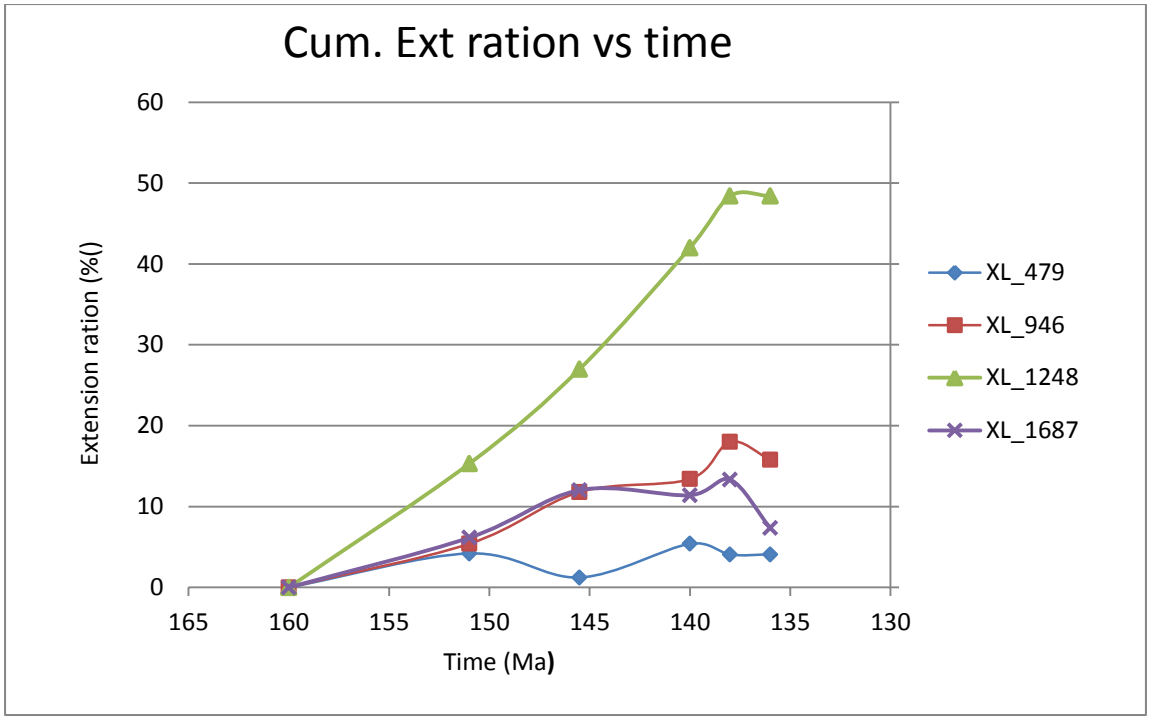

Figure 4.18. Extensional ratio versus time plot.

The positive gradient values in figure 4.15 are an indication of extension while the negative values show compression and the tabulated negative values (Table 4.9 - 4.13) are an indication of compression.

DISCUSSION

INTERPRETATION VALIDATION

The seismic interpretation is considered valid and balanced as the hangingwall and the footwall cut-offs were joined (restored to their undeformed stated) showing a strata thickness that is uniform across the faults on the pre-rift sequence and a thickening hanginwall strata on the syn-rift sequence. Re-interpretation had to be made as some irregularities appeared during the restoration process showing lack of geological sense and a violation of well-known geologic concepts. Examples of the many encountered interpretation errors are shown in figures 4.19 and 4.20.

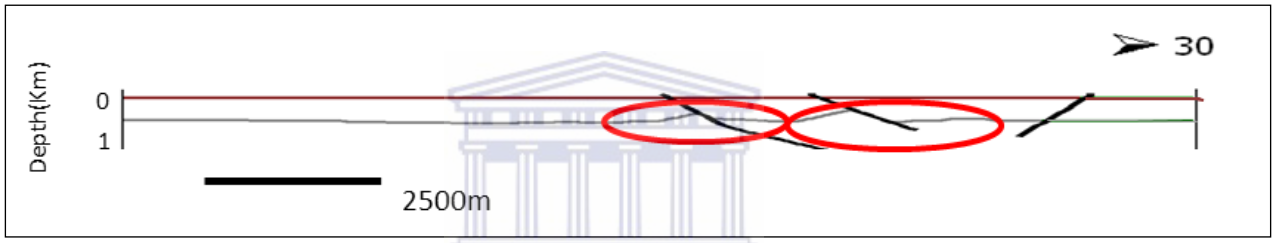

Figure 4.19. Interpretation errors on pre-rift sequence across faults.

In Figure 4.19, the pre-rift sequence across the faults shows a wedging geometry (which is a normal phenomenon on a simplistic model of a growth faults) but is supposed to have uniform thickness. In figure 4.20, the interpreted syn-rift sequence appeared to be thinning on the hanging wall which is contrary to the expected wedging geometry.

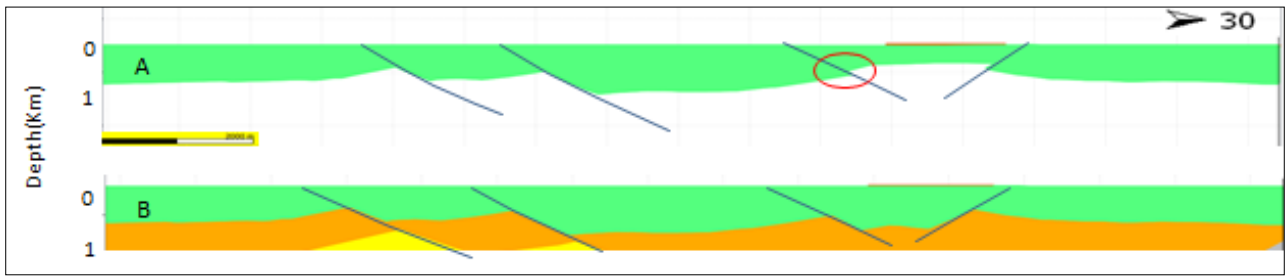

Figure 4.20. An interpretation error that appeared when restoring is shown in cross-section A and cross-section B shows a valid re-interpretation.

Re-interpretation on horizon correlation across the faults was than performed to reduce such interpretation errors as shown in the above figures providing a more valid interpretation, the restored section interpretations are shown in figures 4.11-4.14.

Section restoration also provided insight into the paleo-geometry and structural development through time of the area under study. In Table 4.8 the results show three orders of faulting magnitude activated at different times during rifting, the oldest set of faults are F1, F2 and F5 cutting through the syn-rift and pre-rift sequences alike and are present in all the seismic sections. These faults are ~Late-Jurassic in age and were active throughout the rifting process. The second generation of faults is defined by F3 and F4; these cut through the syn-rift sequence down to the lower shallow marine sediments deposited during the Tithonian and are also present in all the seismic sections. The third generation of faults is defined by F3a and F4a; these are only interpreted in XL_1248 and XL_946 and are much younger as they are cutting through the late syn-rift sequence only and are Late Berriasian in age. The above mentioned fault generation concurs with that described by Van der Merwe and Fouché (1992).

Section line 1687 shows an average extension rate of~ 0.08 mm/year since rifting onset and rifting continued at this rate until the end Kimmeridgian (~151 Ma) after which it gradually increased to ~0.14 mm/year by the end of the Tithonian (145.5 Ma). An inversion episode is recorded to have occurred during the Berriasian (~140Ma) with a total shortening ratio of 0.5 % interposed by continued extension. Another compression followed with a shortening ratio of ~5.3% by End Valanginian-Early Hauterivian (~136).

Restoration of section line 1248 shows no significant occurrence of shortening throughout Basin evolution though (Fig 4.7), but a tectonic inversion that affected the late-syn rift and early post rift sequences is interpreted to have re-activated fault 4. This event is matched to the End Valanginian-Early Hauterivian (~136) compression. The extension in this area is at its maximum and increased from an average rate of 0.18 mm/year since rifting onset to 0.3 mm/year in the Late Valanginian

The extensional rates and ratios of section line 946 are comparable to those of section line 1687 (Figure 4.15) the only difference is the absence of the first compressional phase which was more of a reduction in extensional rate from 0.2 mm/year to 0.05 mm/year.

Section line 479 restorations shows that this part of the basin has experienced a more intense compression and minimal extension.

During Tithonian (~145.5 Ma) the first compressional episode resulted in ~2.8% shortening and the second compressional phase to have started in the Late Valanginian to Early Hauterivian (Table 4.12).

A structural architecture of a simple half *graben* (Figure 4.21) explains why along the cross-line 1248 there is a greater amount of extensional comparative to other section lines, it is because displacement is maximum at the centre of the fault (only the right half of the fault is shown) and decreases towards the fault tips where displacement is at its minimum.

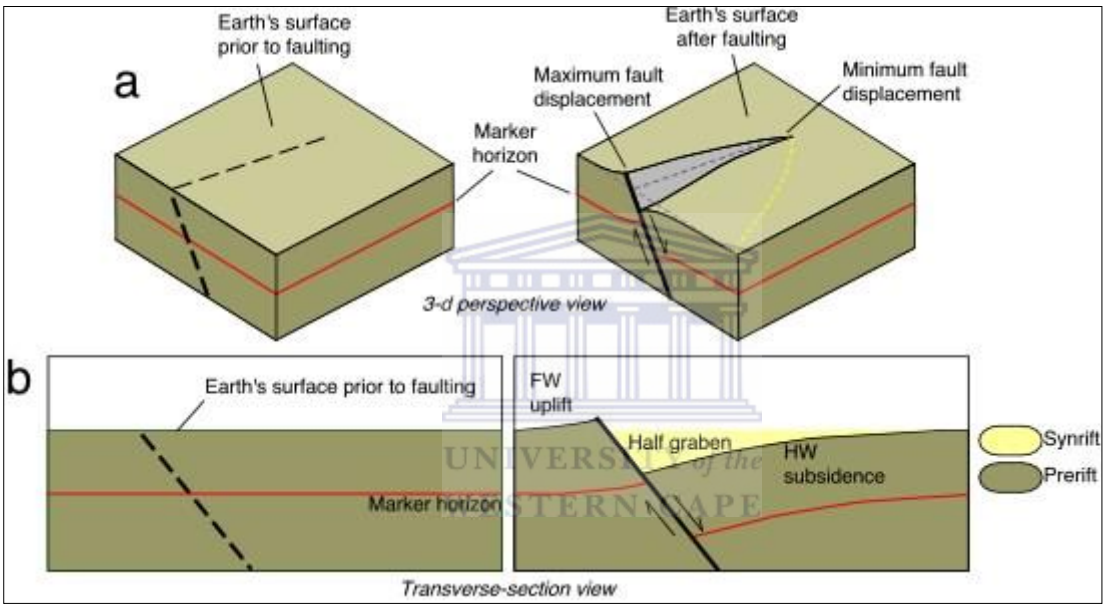

Figure 4.21. Fault-displacement geometry.

Source: http://www.ldeo.columbia.edu/~polsen/nbcp/breakupintro.html

The above phenomenon is not so simple in this regard and has been complicated by inversion resulting to some amount of shortening in the section lines further NW and SE. From the restoration application it can then be seen that this part of the basin formed through an interplay of alternating extensional and compressional phases. This interpretation agrees with Van der Merwe and Fouché's (1992) findings.

Two compressional phases occurred in the most southerly and northerly part of the study field with only one compressional phase in the central part of the study area. The first

compression only affected the syn-rift deposits with the second deforming both the syn-rift and early post rift deposits.

The position of the null point shows the intensity of the inversion and in Figure 4.7 the null point is interpreted along fault 4 plane on the lower bounding horizon of the post-rift sequence showing no significant displacement, this is similar to schematic diagram a) in figure 4.22 and thus the second inversion phase is considerably minor (not complete).

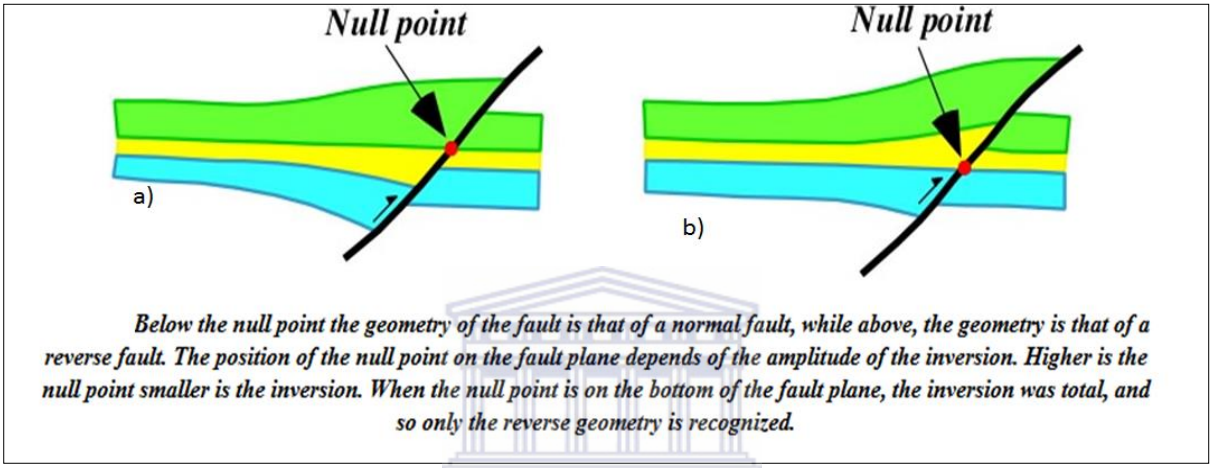

Figure 4.22. Shows the null-point position and its significance on inversion intensity.

Source: http://plate-tectonic.narod.ru/tectonics4photoalbum.html

CONCLUSION AND RECOMMENDATION

The seismic interpretation has been validated using section restoration technique and the structural interpretation of the F-A gas field shows that the area is dominated by low angle listric normal faults with dip values ranging between 19^{o}-35^{o}, these dip in opposite directions forming a conjugate set and whether or not they have a common *decollement* at depth is still unclear and possibly sits at a deeper level (out of the seismic scope). Three depositional sequences are identified viz: the pre-rift strata, the syn-rift strata and the post-rift strata. Therefore further studies on predicting structures outside the seismic scope are still needed which will also aid in understanding which set of faults are synthetic and or antithetic.

Section restoration also revealed the underlying geological structures (masked by the overlying deposits) and their controls. Through a sequential restoration and decompaction process basin evolution and structural development were studied and results from the four interpreted cross-sections show that the syn-rift strata was deposited in a basin subjected to both extension and compression.

Two inversion episodes though minor are concluded based on a ~5.8 and ~3.3 % shortening ratio respectively in the NW and SE part of the study area. The post-rift inversion episode has been interpreted to have re-activated some of the faults. The central part experienced a maximum extension ratio of ~15.8% creating a greater accommodation space and thus thicker sediment accumulations are concentrated along the 1248 cross line and thinning to the NW and SE.

The tectonic implication and the mechanism on the alternating extensional and compressional phases within the basin are still somewhat unclear and some school of thought has proposed two simplistic models which still to date remain a speculation. One model suggests that during fault inactivity, stress built-up occurred in adjacent plates which resulted in compression and extension followed successively by stress release. Another model suggests that the inversion episodes may be as a result of small changes in plate motion during the Western Gondwana break-up (Van der Merwe and Fouche, 1992). In lowering the rate of uncertainty on the structural interpretation, forward modelling should also be formed as a surety that the restored structural model is representative of the present day structural architecture.

BIBLIOGRAPHY

Allen, P. A. & Allen, J. R., 2005. *Basin Analysis: Principlies and Application*, 2nd ed. Malden, USA: Blackwell Publishing Ltd, pp. 349-395.

Ben-Avraham, Z., Hartnady, C.J.H. & Kitqhin, K.A. 1997. Structure and Tectonics of the Agulhas-Falkland Fracture Zone. *Tectonophysics*, 282, 83-98. doi:10.1016/S0040-1951(97)00213-8.

Bidlle, K.T., Uliana, M.A., Mitchum, R.M., Fitzgerald, M.G and Wright, R.C. 1986. The stratigraphic and structural evolution of the central and eastern Megallane Basin, southern South America. In "Foreland Basins", (eds) Allen, P.A and Homewood, P., Int. Assoc. Sediment. Spec. Publ. No. 8, pp. 41-61.

Birch, F., 1961. The velocity of compressional waves in rocks to 10 kilobars, part 2. *J. Geophysics*. Res, 66, pp. 2199–2224.

Broad, D.S., Jungslager, E.H.A., McLachlan, L.R. & Roux, J. 2006. Geology of the offshore Mesozoic basins. In: *The Geology of South Africa* (Ed. by M.R. Johnson, C.R Anhaeusser & R.J. Thomas), pp. 553-571. Geol. Soc. South Africa, Pretoria.

Brown, L.F.Jr., Benson, J.M., Brink, G.J., Doherty, S., Jollands, A., Jungslager, E.H.A., Keenam, J.H.G., Muntingh, A. & Van Wyk, N.J.S. 1995. Sequence stratigraphy, in offshore South African divergent basins. An atlas on exploration for Cretaceous lowland traps by Soekor (Pty) Ltd. Am. Assoc. Pet. Geol. Stud. Geol. 41.

Cartwright, J., 1989. The structural and stratigraphic development of the Gamtoos and Algoa Basins. Volume Soekor Report.

Calvert, A.J., 2004. A method for avoiding artifacts in migration of deep seismic reflection data. doi : 10.1016/j.tecto.2004.07.06.

Cole, D.I. 1992. Evolution and development of the Karoo Basin. *In*: de Wit, M.J. and Ransome, I.G.D. (eds.), Inversion tectonics of the Cape Fold Belt. Karoo and Cretaceous Basin of Southern Africa, Balkema, Rotterdam, pp, 87-100.

Condie, K.C., 1989. 'Plate tectonics and crustal evolution'. Pergamon Press, Oxford, pp. 476.
Dingle, R.V., Siesser, W.G. & Newton, A.R., 1983. Mesozoic and Tertiary Geology of Southern Africa. A.A. Balkema, Rotterdam, pp. 375.

Du Toit, S. R., 1976. Mesozioc geology of the Agulhas Bank, South Africa.

Gibbs, A., 1984. Structural evolution of extensional basin margins. *Journal of the Geological Society of London,* Issue 141, pp. 609-620.

Gibbs, A., 1989. Structural styles in basin formation.. *Mem. Am. Ass. Petrol. Geol.,* Issue 46, pp. 81-94.

Gibbs, A., 1990. Linked fault families in basin formation. *Journal of Structural geology,* Issue 12, pp. 795-803.

Gilbert, D., 1977. Organic facies variation in the Mesozoic South Atlantic. in 'Initial' Reports Deep sea Drilling Project Leg 75''. (eds.), Hay, W.W., Silbuet, J.C et al., Washington (US Govt. Printers Office), pp. 1035-1049.

Jangslager, E.H.A. 1996. The syn-rift of the Bredsdorp Basin. SOEKOR unpubl. Rept. SOE-GEO-RPT. 380, 61p.

Jangslager, E.H.A. 1999. Petroleum habitanats of the Atlantic margin of South Africa. In: Cameron, N.R.., Bate, R.H. and Clure, V.S. (eds.), *The oil and gas Habitants of the South Atlantic.* Spec. Publ. Geol. Soc. London, **153,** pp. 153-168.

Johnson, M.R. 1991. Sandstone petrography, provenance and plate tectonic settings. *In:* Gondwana context of the southern Cape-Karoo Basin. *South African Journal of Geology*, 94, pp. 137-154.

McLachlan, I.R. & McMillan, I.K. 1979. Micro faunal biostratigraphy, chronostratigraphy and history of Mesozoic and Cenozoic deposits on the coastal margin of South Africa. Geokonges 77, Geol. Soc. S. Afr. Spec. Publ., 6, pp. 161-181.

McMillan, I.K., Brink, G.I., Broad, D.S. & Maier, J.J. 1997. Late Mesozoic basins off the south coast of South Africa. In: *Africa Basins* (Ed. by R.C. Selley), pp. 319-379, Elsevier, Amsterdam.

Petroleum Agency SA, 2003. South African Exploration Opportunities, South African Agency for Promotion of Petroleum Exploration and Exploitation, Cape Town, pp. 27.

Petroleum Agency SA, 2004/5. South African Exploration Opportunities, South African Agency for Promotion of Petroleum Exploration and Exploitation, Cape Town, pp. 27.

Petroleum Agency SA, 2013. South African Exploration Opportunities, South African Agency for Promotion of Petroleum Exploration and Exploitation, Cape Town, pp. 27.

Ramsay, J.G. & Huber, M.I., 1987. Folds and Fractures. *The techniques of Modern Structural Geology*. (2), pp. xi+391.

Slater, J.G. and Christie, P.A.E., 1980. Continental strecthing: An explanation of post-mid-Cretaceous subsidence of the central North Sea Basin. *Journal of Geophysical research, 85*, pp. 3711-3739.

Sonibare, W. A., Sippel, J., Scheck-Wenderoth, M. & Mikes, D., 2014. Crustal-scale 3D model of the Western Bredasdorp Basin (Southern South Africa): data based insights from combined isostatic and 3D garvity modelling. *Basin Research,* Volume 0, pp. 1-26. doi: 10.1111/bre.12064.

SOEKOR. 1994a. Orange Basin. *Rep. S. Afri. Licensing Round inf. Brochure,* pp. 18

SOEKOR. 1994b. Outeniqua Basin. *Rep. S. Afri. Licensing Round inf. Brochure,* pp. 55.

Thomson, K. 1998. When did the Falkland rotate? *Mar. Pet. Geol.,*15, pp. 723-736.

Turner, J.R., Grobbler, N., & Sontundu, S., 2000. Geological modelling of the Aptian and Albian sequences within Block 9, the Bredasdorp Basin, offshore South Africa: *Journal of African Sciences*, **31**(1), p. 80.

Van der Merwe, R. & Fouche, J., 1992. Inversion tectonic in the Bresdasdorp Basin, offshore South Africa.

Yamada, Y., & McClay, K., 2003. Application of Geometric Models to Inverted Listric Fault Systems in Sandbox Experiments. Paper-1: 2D Hangingwall Deformation and Section Restoration. Journal of Structural Geology. 25, pp.1551-1560

Null point and its significance on inversion intensity schematic diagram, Source : http://plate-tectonic.narod.ru/tectonics4photoalbum.html.

Fault-displacement geometry, Source:
http://www.ldeo.columbia.edu/~polsen/nbcp/breakupintro.html

APPENDIX A

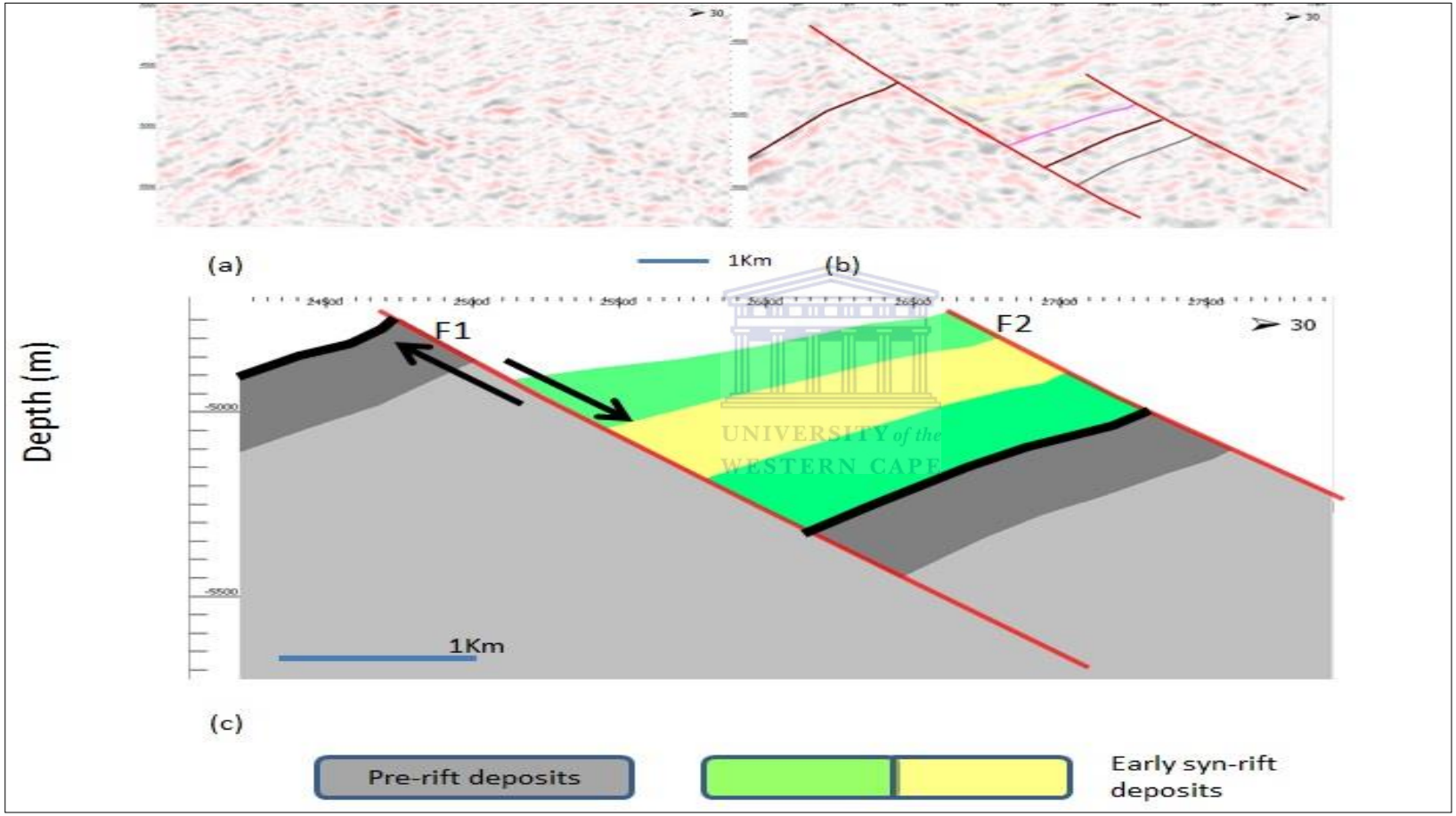

Figure 4.5 (a) seismic section showing rift-onset (b) interpretation of rift onset unconformity and (c) shows a schematic section from the interpretation.

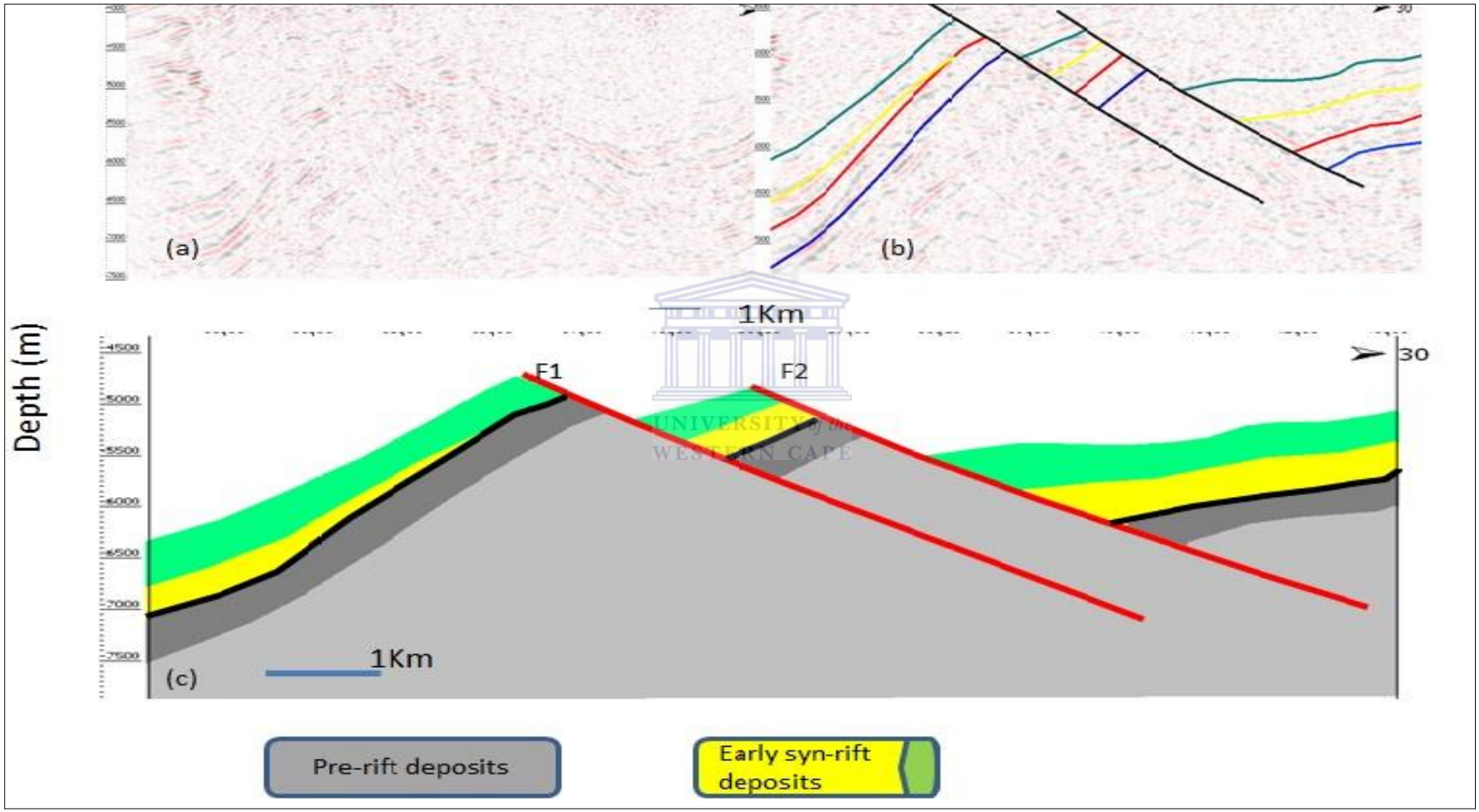

Figure 4.6 (a) and (b) Seismic section showing the correlated rift on-set unconformity and early syn-rift deposits. (c) Shows a schematic section.

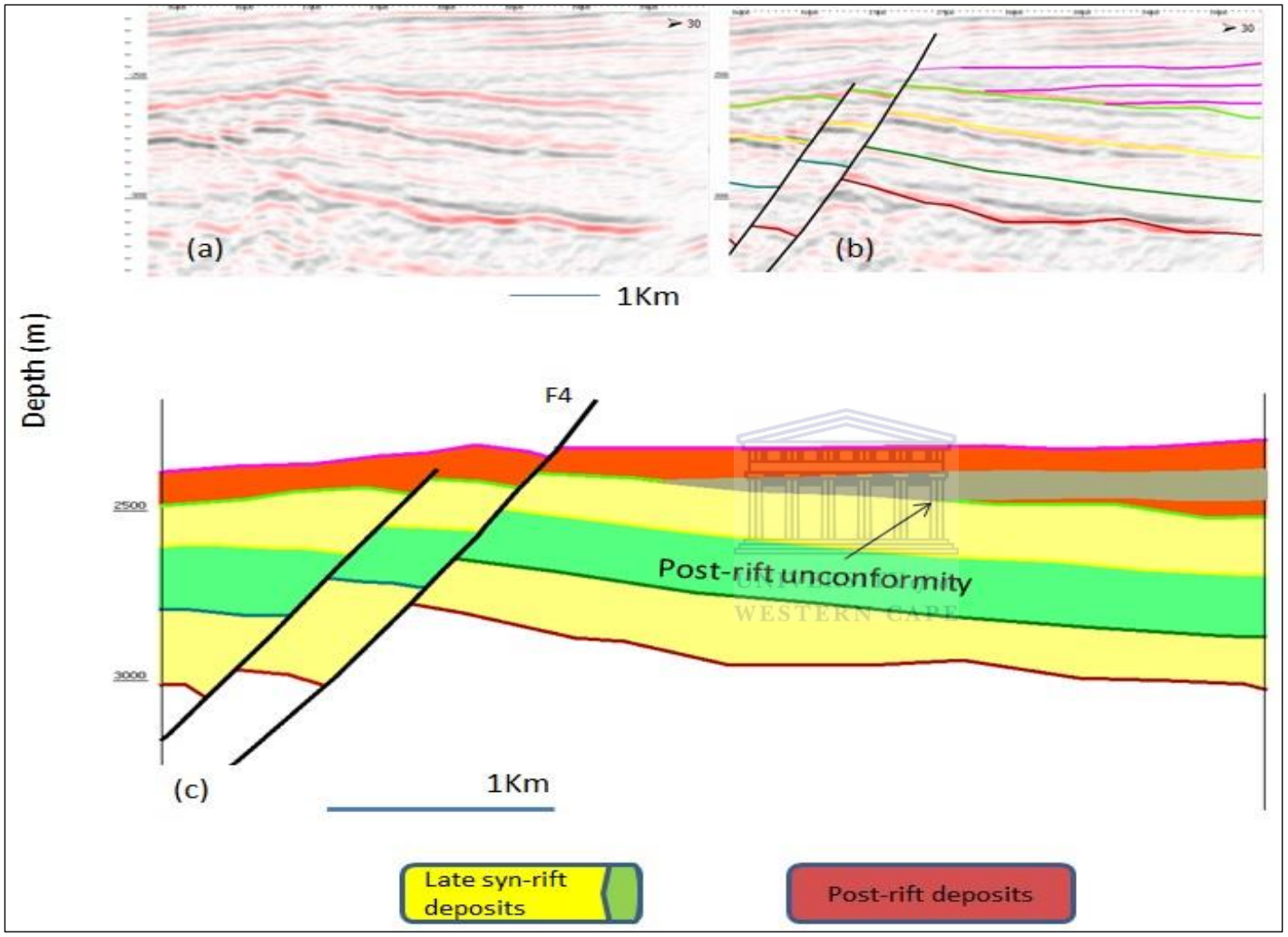

Figure 4.7(a) and (b) shows interpretation of the end of rifting marked by an unconformity and (c) is the schematic section

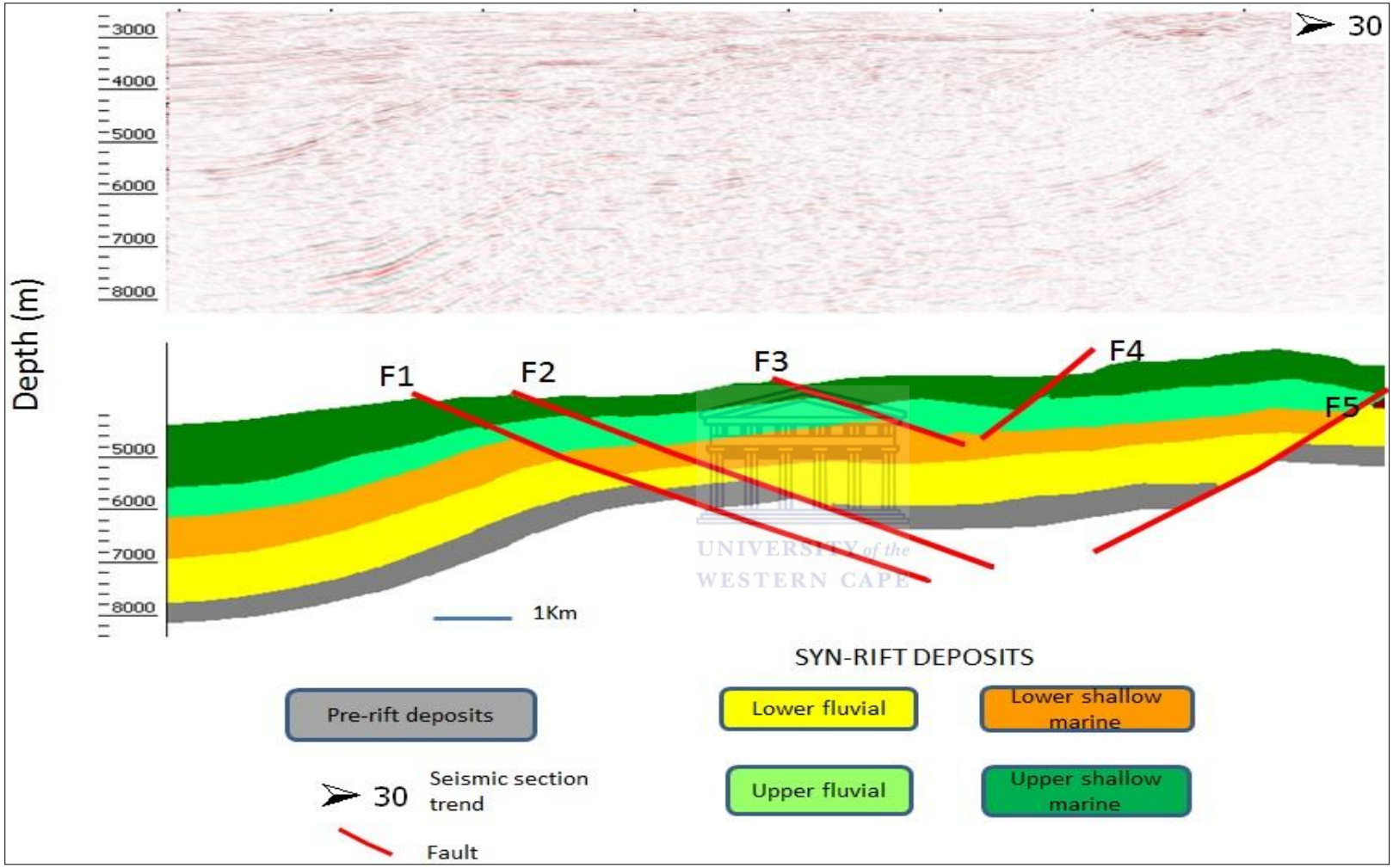

Figure 4.9-Seismic section line 1687 interpretation

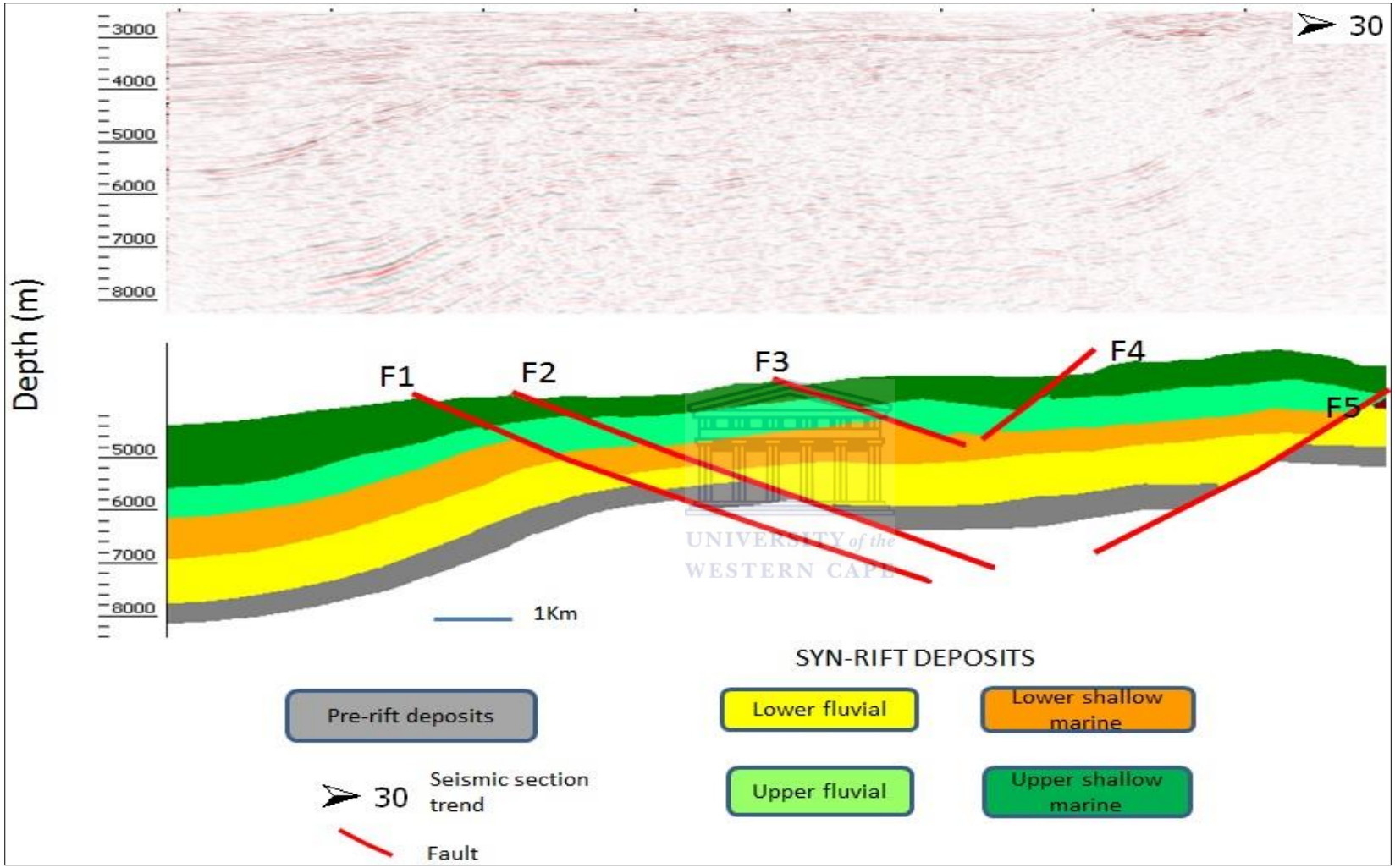

Figure 4.10-Seismic section line 1248 interpretation

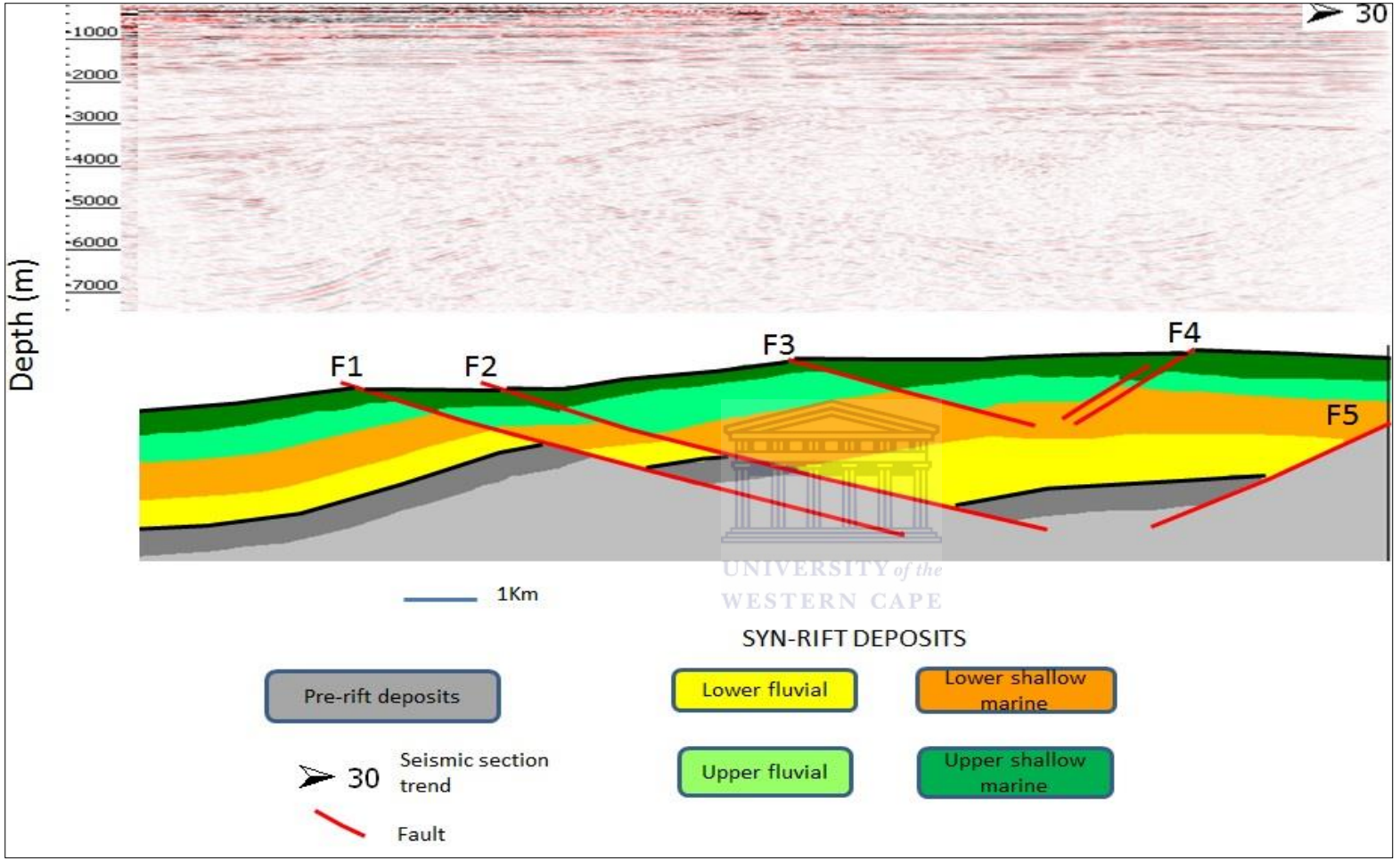

Figure 4.11-Seismic section line 946 interpretation

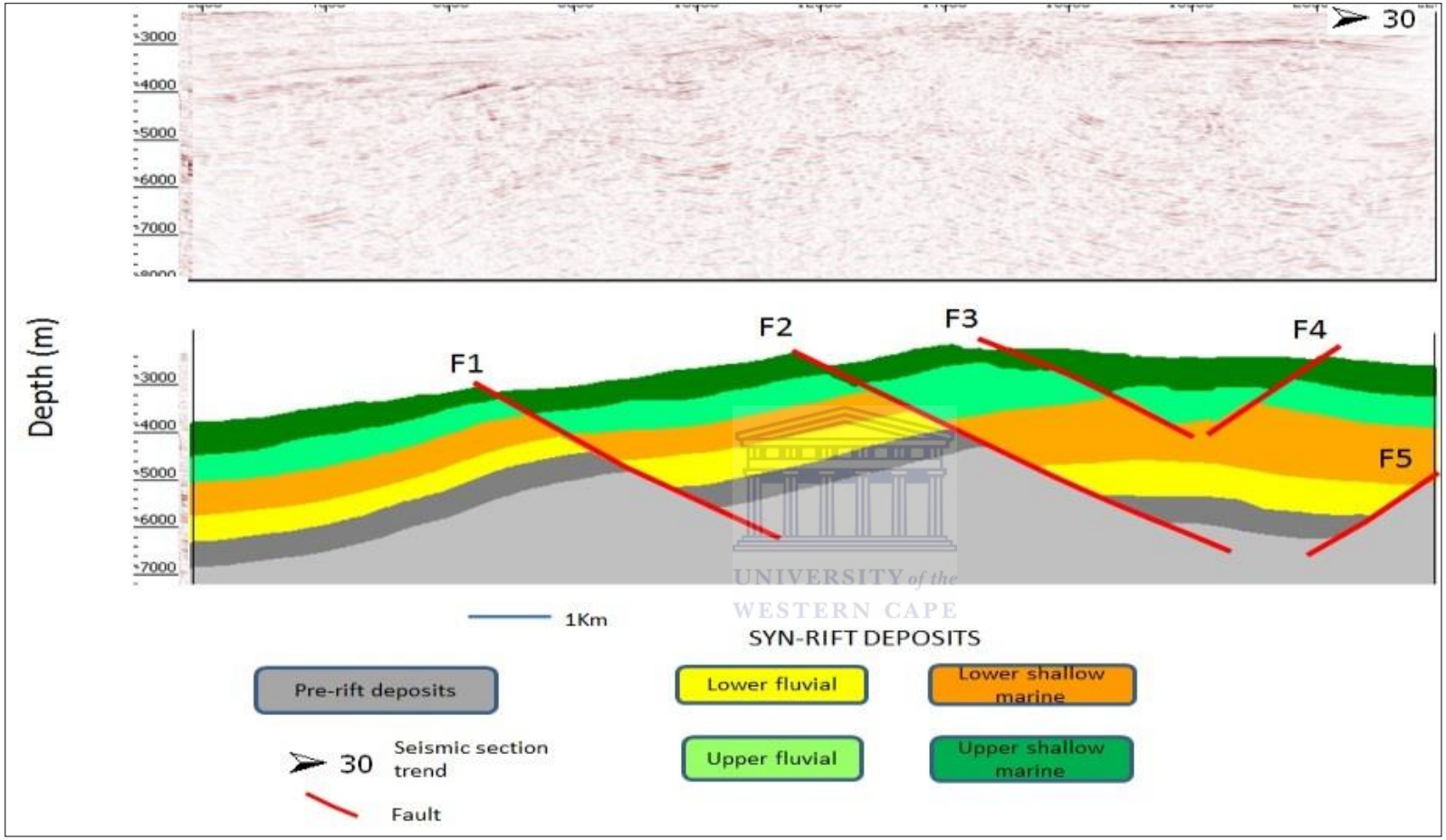

Figure 4.12-Seismic section line 479 interpretation

UNIVERSITY of the
WESTERN CAPE